Received: 26 September 2022 | Revised: 23 January 2023 | Accepted: 5 March 2023

DOI: 10.1111/jfr3.12901

ORIGINAL ARTICLE

CIWEM Chartered Institution of Water and Environmental Management | Journal of Flood Risk Management | WILEY

Importance of catchment hydrological processes and calibration of hydrological-hydrodynamic rainfall-runoff models in small rural catchments

Amrei David[1] | **Ernesto Ruiz Rodriguez**[2] | **Britta Schmalz**[1]

[1]Department of Civil and Environmental Engineering, Chair of Engineering Hydrology and Water Management (ihwb), Technical University of Darmstadt, Darmstadt, Germany

[2]Department of Architecture and Civil Engineering, Chair of Hydraulic Engineering and Water Management, RheinMain University of Applied Sciences, Wiesbaden, Germany

Correspondence
Amrei David, Department of Civil and Environmental Engineering, Chair of Engineering Hydrology and Water Management (ihwb), Technical University of Darmstadt, Franziska-Braun-Straße 7, 64287 Darmstadt, Germany.
Email: a.david@ihwb.tu-darmstadt.de

Abstract

In recent years, many two-dimensional (2D) hydrodynamic models have been extended to include the direct rainfall method (DRM). This allows their application as a hydrological-hydrodynamic model for the determination of floodplains in one model system. In previous studies on DRM, the role of catchment hydrological processes (CaHyPro) and its interaction with the calibration process was not investigated in detail. In the present, case-oriented study, the influence of the spatiotemporal distribution of the processes precipitation and runoff formation in combination with the 2D model HEC-RAS is investigated. In a further step, a conceptual approach for event-based interflow is integrated. The study is performed on the basis of a single storm event in a small rural catchment (low mountain range, 38 km^2) in Hesse (Germany). The model results are evaluated against six quality criteria and compared to a simplified baseline model. Finally, the calibrated improved model is contrasted with a calibrated baseline model. The results show the enhancement of the model results due to the integration of the CaHyPro and highlight its interplay with the calibrated model parameters.

KEYWORDS

2D hydrodynamic modeling, calibration, direct rainfall modeling, hydrological processes, radar data, runoff formation

1 | INTRODUCTION

The rain-on-grid method, also known as direct rainfall modeling (DRM) has become the state of the art for storm hazard analysis in urban and rural catchments (Cea & Rodriguez, 2016; Costabile et al., 2021; David & Schmalz, 2020). In this method, a two-dimensional (2D) hydrodynamic model is applied as a 2D hydrologic–hydrodynamic rainfall-runoff model (HHDRRM). The advantage of the modeling method is that hydrological processes are considered together with the hydrodynamic floodplain flow routing in one modeling system. The method can be applied to determine inundation areas caused by storm events within the entire catchment area (David & Schmalz, 2020). The size of the catchments, in which the DRM is applied, varies considerably. So does the spatial variability of the distribution of hydrological input parameters and the subsequent calibration routine. For

catchments with predominantly agricultural or forestry land use, the catchment size varies from 4 km^2 (Cea & Bladé, 2015) to 185 km^2 (Hall, 2015). For catchments with more mixed and urban land use, the size varies even more from 0.049 km^2 (Fraga et al., 2016) to 232 km^2 (Zeiger & Hubbart, 2021). In David and Schmalz (2021), examples with applications of the rain-on-grid method were compared with focus on how the spatial discretization of the computational mesh and topography took place in the modeling process. A detailed sensitivity analyses was conducted in the study with focus on the interaction of computational mesh and underlying subgrid.

The integration of catchment hydrological processes (CaHyPro) has been established within the framework of spatially distributed hydrological modeling (Guse et al., 2019). There are different spatial scales in which hydrological modeling has evolved. The development went from the original lumped or subcatchment based modeling approach over the so-called semi-lumped models over HRUs to fully 2D distributed models (Guse et al., 2019). Meanwhile, in the field of hydrological modeling, a large number of applications exists for the spatially distributed representation of hydrological processes. Well-known modeling systems in the German-speaking area are, for example, RoGeR, WaSiM-ETH, NASIM or SWAT (Guse et al., 2019).

In the field of 2D hydrodynamic modeling, the DRM has evolved over the past decade due to increased computational power. The analysis of 20 applications with DRM by David and Schmalz (2021) showed that the integration and spatiotemporal resolution of CaHyPro using DRM varies considerably. Two of the studies use radar data as input data. Half of the studies use gauging station data, but only four studies consider spatially distributed rainfall data. In terms of runoff formation, seven studies use a method with spatially distributed runoff coefficients and nine use a spatially uniform runoff coefficient. In six of the studies, the temporal variation of the runoff coefficient during the event was integrated. None of the studies evaluates event related fast interflow as component of the runoff hydrograph. The state of the art of the calibration of the DRM is summarized as the following. The fully integrated method implies that hydrological and hydrodynamic processes are modeled and calibrated in one modeling system together. Here, a parameter based calibration technique of the dominant processes and parameters (mostly roughness and infiltration values) takes place. Examples can be found in Fraga et al. (2016), Jia et al. (2019), and Yu and Coulthard (2015). The method of effective rain-on-grid modeling instead implies that effective precipitation is set as input variable directly to the 2D model. The hydrological parameters, respectively, the effective rainfall rates, are determined externally via a separate modeling system or a simplified infiltration approach. Examples of this approach can be found in Hall (2015), Zeiger and Hubbart (2021), or David and Schmalz (2020). Here, the calibration takes place in two separate model systems.

The internationally used 2D hydrodynamic model HEC-RAS has the capability for rain-on-grid modeling with spatially homogeneous effective precipitation since 2016 (HEC, 2016). With the version 6.0 (2021) there is the possibility of an integrated routine for runoff formation as well as spatially distributed rainfall (HEC, 2020).

If the rain-on-grid model does not take into account the spatiotemporal heterogeneity of CaHyPro, processes that are not actually implemented in the modeling structure might be induced by the calibration of free model parameters of other processes. An example can be that precipitation volumes are adjusted by calibrating the parameters of the runoff formation routine (e.g. SCS-CN values). These parameters may not need to be calibrated if radar rainfall was used as input data. The process of subsurface stormflow or fast event-based interflow can be mentioned as another example. The process can contribute significantly to the runoff event (Weiler et al., 2005). The time to maximum discharge in the model is too short compared to the measured discharge curve. This can be related to the event-dependent interflow. If the process is not included in the model, the modeler might increase the surface roughness values to produce the delay in the runoff hydrograph.

To highlight this problem, the following study investigates the importance of CaHyPro and its interaction with the subsequent calibration routine together with the meanwhile widely used DRM. The question is how a stepwise integration of CaHyPro influences the model results and the final parametrization using the 2D hydrodynamic model HEC-RAS as HHDRRM.

2 | OBJECTIVES

The objective of the study is to analyze the importance of different levels of spatiotemporal representation of CaHyPro with the application of DRM in a small rural catchment. In order to elaborate the respective effect of the integration of CaHyPro, a method should be developed that allows a step-by-step investigation. As a result, a résumé should be drawn on the importance of CaHyPro and its interaction with the calibration process in combination with the DRM. Besides the hydrological scientific investigation of the integration of CaHyPro, the study serves to gain experience with the new technical possibilities of HEC-RAS 6.0 (HEC, 2021). For this purpose, technical issues of the processing of radar data in the GIS should be addressed. A simplified approach for the

calculation of storm-related interflow based on the parallel cascades of linear reservoirs is proposed. The summarized objectives are the following:

- To develop a methodology which allows a step-by-step investigation of the impact of the integration of CaHyPro and its interplay with the calibrated model parametrization together with the DRM in a small rural catchment.
- To integrate radar rainfall, spatially distributed process of runoff formation and a simplified, conceptual approach of interflow to HEC-RAS 6.0.
- To give a résumé on the impact of spatiotemporal resolution of CaHyPro, its interaction with the calibration process and the final model parametrization.

The study is conducted as a case study in the Fischbach catchment. The catchment is part of the field observatory of the Chair of Engineering Hydrology and Water Management (Fachgebiet Ingenieurhydrologie und Wasserbewirtschaftung [IHWB]) from Technical University of Darmstadt (see details in David & Schmalz, 2021; Grosser & Schmalz, 2021; Scholand & Schmalz, 2021; Kissel & Schmalz, 2020; Schmalz & Kruse, 2019).

3 | MATERIALS AND METHODS

3.1 | Project area of Fischbach catchment

The Fischbach catchment has a total area of 38 km^2 (Figure 1). It is part of the Gersprenz river system and is located in the Odenwald region of Hesse in Germany. 93% of the catchment area is covered by a state gauge from which discharge is available since 1985 in a time interval of 15 min (HLNUG, 2020b). These are supplemented by water level observations with 5 min intervals since 2018 from IHWB (2020). Within the catchment area, a flood retention basin with a capacity of 220,000 m^3 was built in the year 2016 (in operation since 2017). The elevations of the watershed range from 592 to 158 masl (mean 283 masl). A terrain model with a resolution of 1 m is provided from HVBG (2017). The CORINE land cover (CLC) (EEA, 2016) is available as land use data and supplemented by the local ATKIS landuse data set (Amtliches Topographisch-Kartographisches Informationssystem [ATKIS]) (HVBG, 2017). The catchment area is predominantly rural with 43.8% agricultural and farmland, 46.3% forest area, and 9.6% areas belonging to settlements including buildings

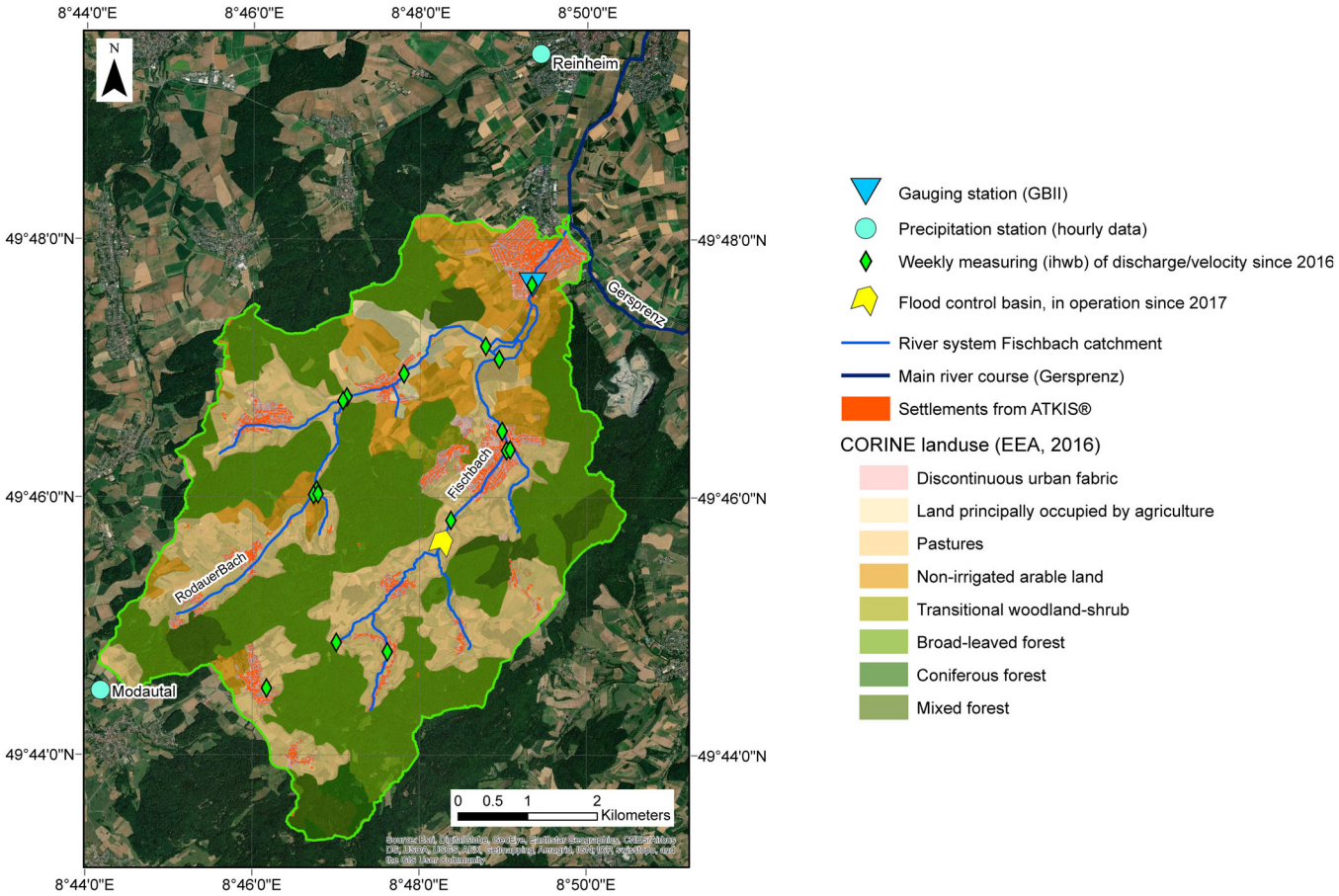

FIGURE 1 Project area of Fischbach catchment in Central Germany (38 km^2).

and roads. As precipitation data, the two nearby precipitation stations of Modautal–Brandau–Kläranlage (HLNUG, 2020a) and Reinheim (Deutscher Wetterdienst [DWD], 2020) are applied. For the respective model extensions, the radar data (RADOLAN-YW) from Winterrath et al. (2018b) with 5 min temporal and 1 km × 1 km spatial resolution is used. For soil data, the official soil map with a scale of 1:50,000 from HLNUG (2017) is taken. As there are no sewage treatment plants in the catchment area, no drainage system was integrated into the model.

3.2 | Rainfall event of April 23, 2018

The observed rainfall event occurred on April 23, 2018. The precipitation station of Modautal–Brandau–Kläranlage recorded a total precipitation sum of 29.2 mm from 3:00 p.m. to 4:00 p.m. According to the official German storm hazard statistics of KOSTRA-2010R (DWD, 2017), this corresponds to a return period of 4 years. The precipitation station of Reinheim recorded a total height of 11.3 mm in the period between 3:00 p.m. and 4:00 p.m. The radar precipitation data have maximum values of 52 mm in the period between 3:00 p.m. and 4:00 p.m. At the gauge of Groß-Bieberau 2 (GB2), the observed discharge increased to a level of 12.5 m^3/s. This corresponds to a return period of 10 years (David & Schmalz, 2020). As a result of the event, flooding occurred on the slopes, on the forest trails and there was flooding of private buildings, bridges and roads (Bickelhaupt, 2018) (Figure 2).

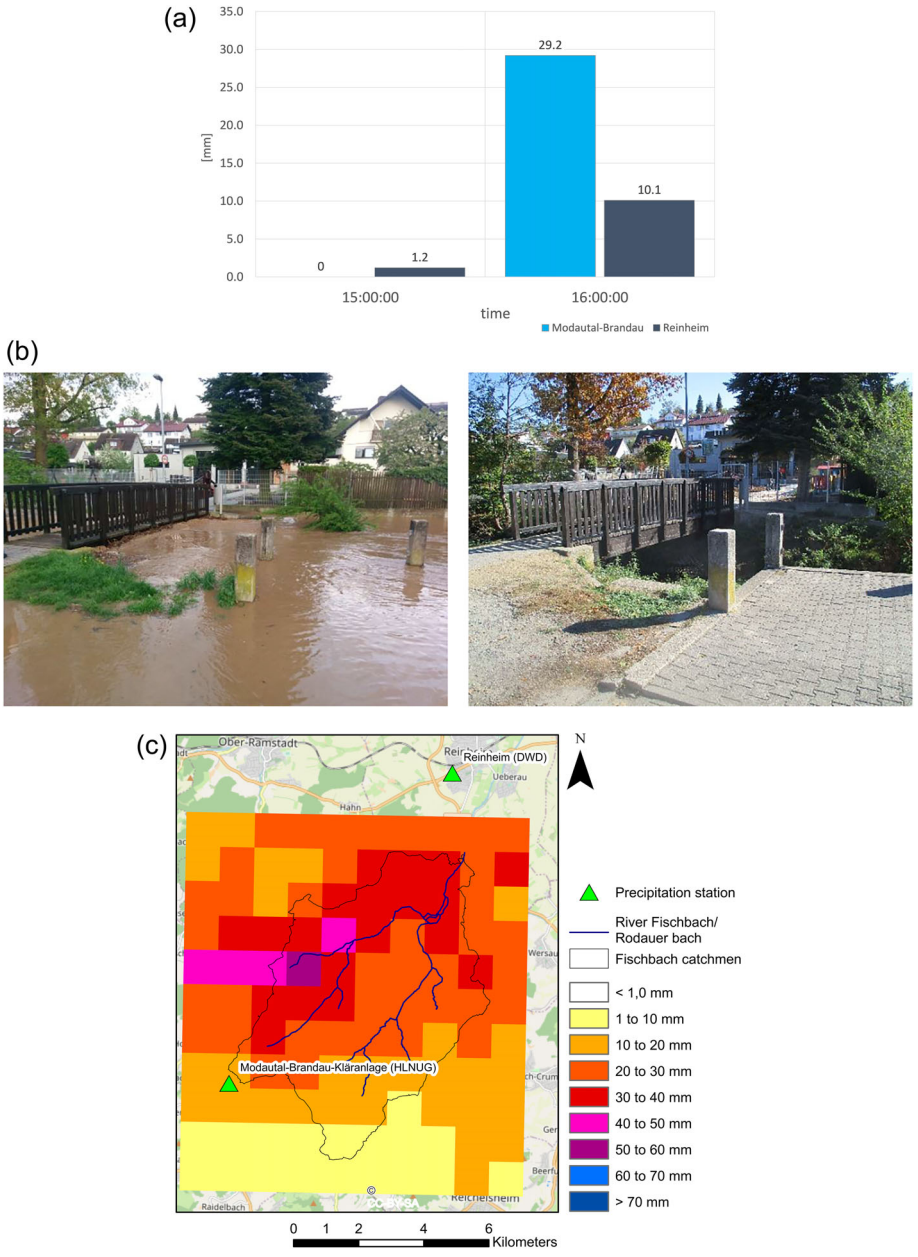

FIGURE 2 (a) Recorded precipitation data at the precipitation stations of Modautal–Brandau–Kläranlage and Reinheim of the April 23, 2018, (b) flooded areas in the village of Groß-Bieberau (Fischbach) near the gauging station GB2, (c) recorded radar rainfall event from the April 23, 2018 with pixel-based accumulated rainfalls sums based on 1 km × 1 km DWD Radolan Raster (Winterrath et al., 2018a).

3.3 | 2D hydrodynamic model HEC-RAS

The 2D hydrodynamic model HEC-RAS is used as HHDRRM in this study. The free model was extended in 2016 with the model version 5.0 (HEC, 2016) by the 2D hydrodynamic solution of the shallow water equations. Furthermore, the possibility of DRM was added to the model capabilities. In the year 2021 (HEC, 2021) with model version 6.0, the model was extended by spatially distributed precipitation input and three different loss methods. The model is used in numerous scientific publications worldwide. Examples on the use of HEC-RAS as HHDRRM can be found in Rangari et al. (2019), David and Schmalz (2020), Zeiger and Hubbart (2021) and Costabile et al. (2021). The technical details and mathematical principles of HEC-RAS are documented in the Technical Reference Manual (HEC, 2020).

3.4 | Iterative model improvement via CaHyPro

The introduced method of iterative model improvement via CaHyPro (IMI-CaHyPro) carried out here involves the application of DRM together with HEC-RAS based on an observed storm event on April 23, 2018. A schematic overview of the method can be found in Figure 3. In the first part, a simplified model (*Baseline model*) is set up in HEC-RAS as a reference model. This contains a common model set-up with simplified implementation of CaHyPro. The model is calibrated using observed discharge time series available for the project area (HLNUG, 2020b). The calibration of the baseline model takes place as parameter based calibration via SCS-CN values (−) for the runoff formation and Manning's n values ($s \times m^{-1/3}$) for the runoff concentration. In the second part, the hydrological processes of precipitation, runoff formation and event-related interflow are iteratively improved and added to the HEC-RAS baseline model. The integration of CaHyPro takes place successively. The model improvement is conducted in HEC-RAS. In order to accurately study the effect of each added hydrologic process, they are added stepwise before the actual calibration is performed. The following model improvements were made:

1. Precipitation
   1.1 1 h radar data
   1.2 5 min radar data
2. Runoff formation
   2.1 Spatial SCS-CN values
   2.2 Spatiotemporal SCS-CN values
3. Interflow
   3.1 Catchment based
   3.2 Subcatchment based.

The improved model (*IMI-CaHyPro model*) is then calibrated using the parameters of runoff formation (SCS-CN values), event related interflow (storage coefficients k_2 [h]) and runoff concentration (Manning's n values [$s \times m^{-1/3}$]).

Subsequently, (a) the model results of the uncalibrated baseline model and the modified model set-ups are compared, (b) the influence of the approach of IMI-

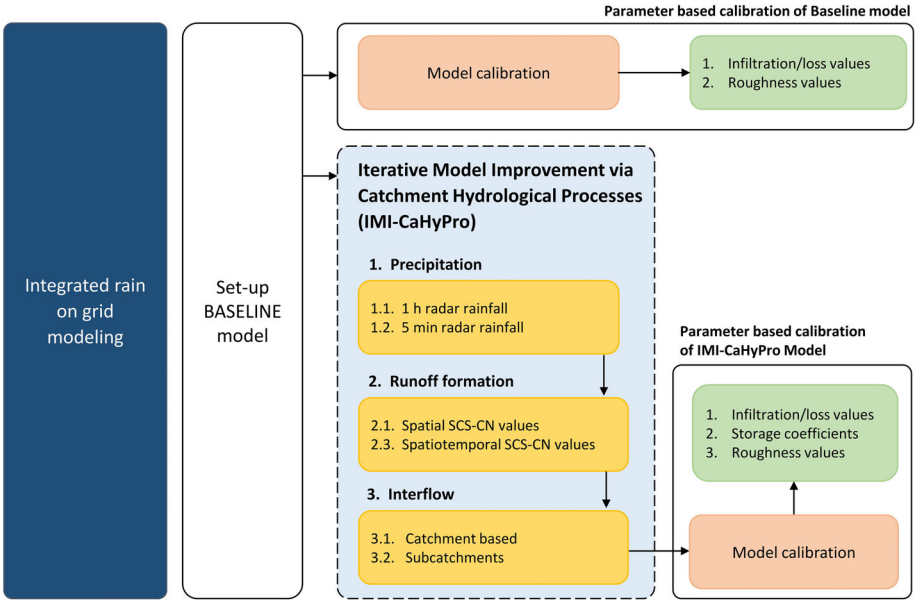

FIGURE 3 Overview of the Iterative Model Improvement via catchment hydrological processes (IMI-CaHyPro).

CaHyPro on model parametrization is discussed, and (c) a general conclusion is drawn on the integration of CaHyPro in combination with the application of DRM.

In the following, the technical details of the baseline model and the stepwise model improvements for the processes of precipitation, runoff formation, and interflow processes of the IMI-CaHyPro approach will be explained.

3.5 | Baseline model

The model area (38 km^2) is spatially discretized with a computational grid with 5 m resolution. According to David and Schmalz (2021) this corresponds to the coarsest recommended resolution for the application of DRM and is still acceptable with regard to the computational times. The underlying terrain geometry ('subgrid'; Casulli, 2009) is defined with a resolution of 1 m. The river course is burned into the model domain using supplementary terrestrial cross-section surveys (David & Schmalz, 2020). The time step is set to 1 s for numerical solution of Diffusion Wave approximation and expected maximum velocities of 5 m/s in the catchment. By this time step selection the Courant criteria with CFL ≤1 is fulfilled. The selected time step is within the recommendations of Rangari et al. (2019) and David and Schmalz (2020) for applications of DRM together with HEC-RAS. The model area is assigned roughness values (Manning's n values) for surface runoff according to Downer and Ogden (2006) and for channel flow according to Patt and Jüpner (2013). SCS-CN values using the SCS method from USDA (1986) are assigned according to Deutscher Verband für Wasserwirtschaft und Kulturbau e.V (DVWK) (1984) and USDA (1986, p. 55). For the model, a mean SCS-CN value is determined for the entire catchment area. Precipitation data from the two precipitation stations (Figure 2) with an hourly time interval are used. Interpolation between the stations is done using Thiessen polygons. The following Figure 4 shows the total and effective input precipitation of the baseline model.

3.6 | Technical implementation of iterative model improvement

3.6.1 | Precipitation

One hour radar rainfall

As model extension (Precipitation I), precipitation is integrated to the model domain as spatially distributed precipitation data. For this purpose, the data set is integrated as a grid with an hourly resolution (Figure 5a). The 5 min radar data from Winterrath et al. (2018b) was aggregated to hourly input data to get time-consistent time-intervals as for the precipitation station

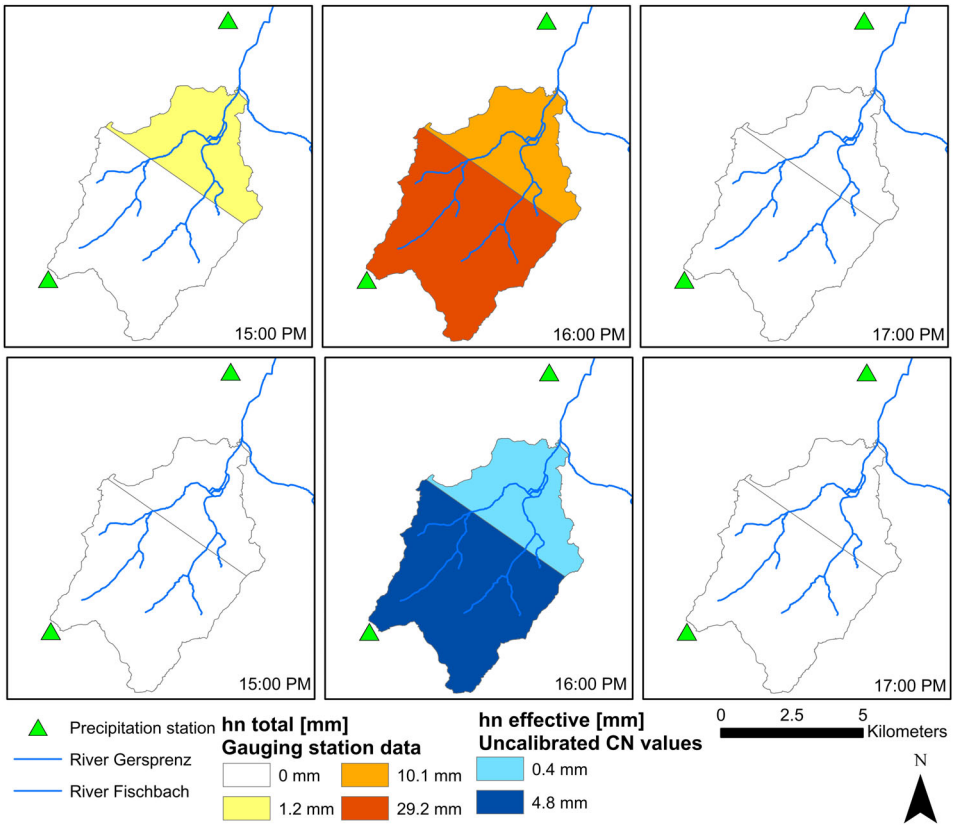

FIGURE 4 Precipitation input for April 23, 2018 of baseline model with Thiessen–Polygons and averaged CN-value for total (above) and effective (below) precipitation.

data of the baseline model. The general preprocessing for the creation of the input data is performed using ArcGIS. The original data set is available for each time step as *.ascii-file for the whole of Germany in a polar stereographic coordinate system. This is first converted as *.tif-file and then projected into the project-related coordinate system (UTM) via GIS. The resulting data set is cut out with the model area and reconverted as *.ascii-file. The conversion tool ("asc2dss.exe") from HEC (HEC, 2017) is used to convert each *.ascii-file into a *.dss file. The *.dss file is imported into HEC-RAS as precipitation input data set. The technical details are presented in (HEC, 2017).

Five minutes radar rainfall

For the next model extension, 5 min radar rainfall time series from Winterrath et al. (2018b) are created as input data instead of hourly rainfall data (Figure 5b).

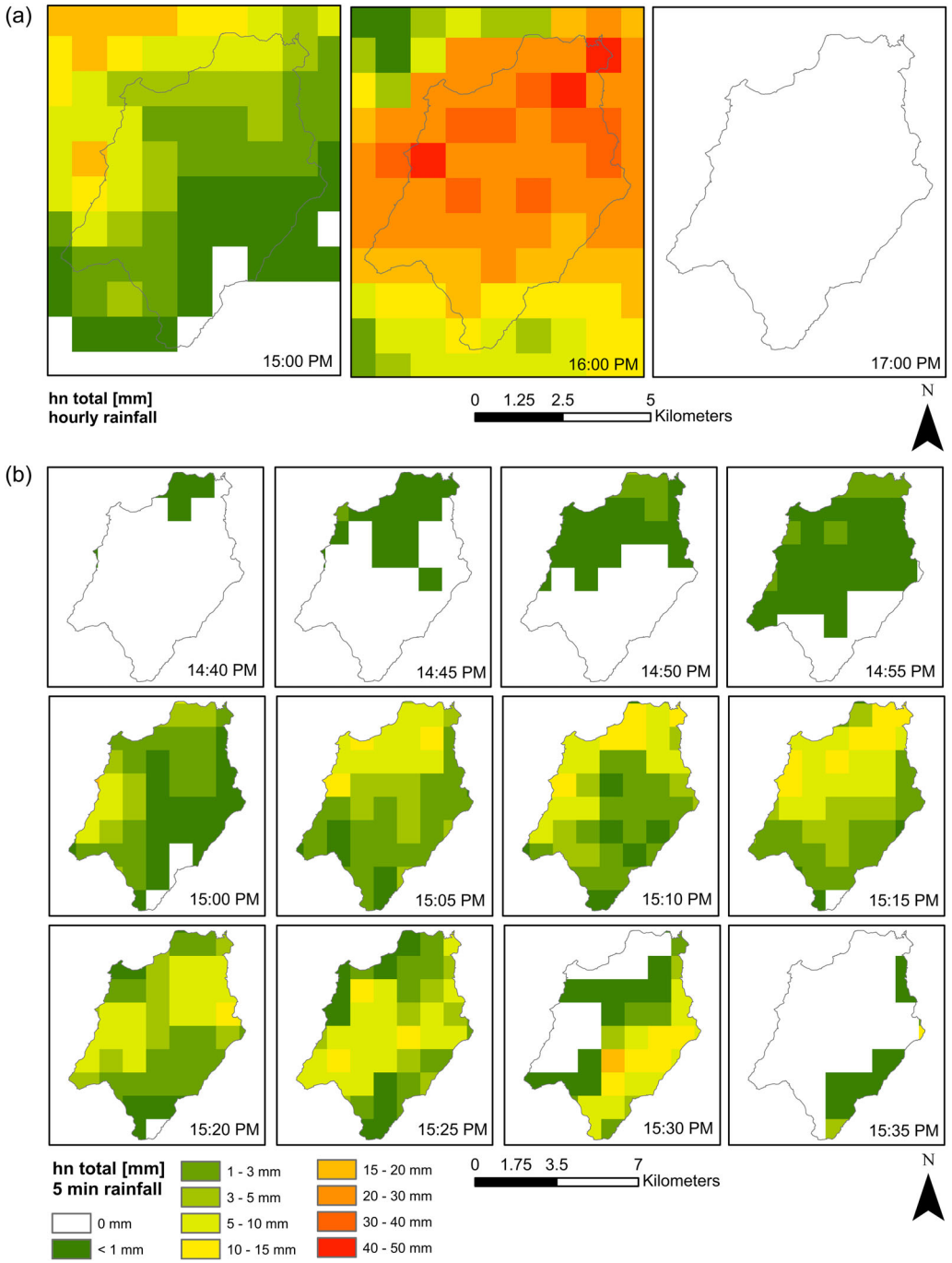

FIGURE 5 Gridded precipitation data: (a) Hourly precipitation input for April 23, 2018 based on Winterrath et al. (2018a), (b) 5 min precipitation input for April 23, 2018 based on Winterrath et al. (2018b).

3.6.2 | Runoff formation

Spatial SCS-CN values

As further model extension, spatially distributed CN values were added to the model area. This results in a cell-by-cell calculation of runoff coefficients depending on the individual land use and soil classes (Figure 6). Time invariable runoff coefficients were calculated based on rainfall sums of each cell applying the widely used SCS-CN method (USDA, 1986, p. 55). The underlying equations are presented in Equations (1)–(3). The resulting effective precipitation rates in Figure 7.

$$h_{n,\ \text{effective}} = \frac{(h_{n,\ \text{total}} - I_a)^2}{(h_{n,\ \text{total}} - I_a) + S_{\max}} \tag{1}$$

$$S_{\max} = \frac{25400}{CN} - 254 \tag{2}$$

$$I_a = a * S_{\max}, a = 0.05 \tag{3}$$

where $h_{n,\text{effective}}$ is the effective precipitation height (mm), $h_{n,\ total}$ is the total precipitation height (mm), I_a is the initial abstraction (mm), $S_{\max}$ is the potential maximum retention (mm), a is the constant to determine initial abstraction; $a = 0.05$ (DWA, 2008).

Spatiotemporal SCS-CN values

For the next model improvement, the temporal distribution of the runoff formation process during the precipitation event is considered (Figure 8). For this purpose an extended version of the SCS-CN method (Zaiß, 1989 as cited in DWA, 2008) is used. This method recalculates the runoff coefficient after each time step for the accumulated rainfall sum instead of a constant value for the entire event (Equation 4). The total rainfall raster is then multiplied with the runoff coefficient for each time step (Equation 5). The original method by Zaiß (1989) additionally includes the initial soil moisture condition in the determination of the SCS-CN values. This was not integrated in the routine here since the impact of the initial state of the catchment is not focused on in this study.

$$\psi_i = 1 - \left(\frac{I_a}{0.05 * \sum h_{ni} + 0.95 * I_a}\right)^2 \tag{4}$$

$$h_{n,\text{effective},i} = \psi_i * h_{ni} \tag{5}$$

ψ_i is the runoff coefficient for each timestep, h_{ni} is the total rainfall height for each timestep (mm); $h_{n,effective,i}$ is the effective rainfall height for each timestep (mm).

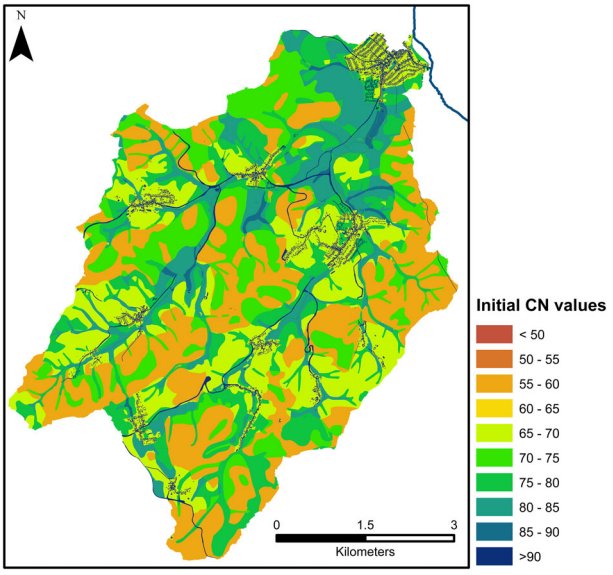

FIGURE 6 Spatially distributed CN-values based on the different soil (HLNUG, 2017) and landuse (EEA, 2016; HVBG, 2017) categories.

3.6.3 | Interflow

A simplified procedure based on two parallel cascades of linear reservoirs is used to obtain the event-based interflow (Becker & Glos, 1969 as cited in Wackermann, 1981). The conceptual hydrological approach assumes that the direct runoff can be divided into a fast and a slow cascade via two different storage coefficients (k_1, k_2) (DWA, 2008). Even though the simplified conceptual approach with two different storage times does not allow 1:1 transferability on the corresponding physical hydrological components, the slower cascade will be defined in the following as fast, event-based interflow. HEC-RAS computes surface roughness on a cell-by-cell basis, resulting in runoff retention. It is difficult to add another subsurface runoff component on a cell-by-cell basis with the existing model set-up. Therefore, as a first model extension (Interflow I) a catchment based simplified approach was implemented. As a second extension (Interflow II) interflow is added via subcatchments to the model area. The following equations (Equation 6–13) based on DWA (2008) and Wackermann (1981) are used to determine (sub-) catchment based interflow.

$$U(t) = \alpha * \frac{t}{k_1^2} * e^{\frac{-t}{k_1}} + (1 - \alpha) * \frac{t}{k_2^2} * e^{\frac{-t}{k_2}} \tag{6}$$

$$k_1 = \frac{0.555}{\frac{L}{\sqrt{J}}^{0.61}} + 0.5111 * \ln\frac{L}{\sqrt{J}} - 0.355 \tag{7}$$

$$k_2 = 3 * k_1^{1.3} \tag{8}$$

$$\alpha = 1 - 0.02425 * \left(\ln \frac{L}{\sqrt{J}}\right)^{3.2444}, \frac{L}{\sqrt{J}} \leq 10\,\text{km} \tag{9}$$

$$\alpha = \frac{3.91}{\left(\frac{L}{\sqrt{J}}\right)^{0.86}} + 0.1, \frac{L}{\sqrt{J}} > 10\,\text{km} \tag{10}$$

$$k_1^* = 4.38 - 2.25 * ChDe \tag{11}$$

$$k_2^* = 0.0168 * \frac{L}{\sqrt{J}} + 2.5 \tag{12}$$

$$\alpha^* = 0.323 * e^{-0.00765 * \frac{L}{\sqrt{J}}} \tag{13}$$

*For catchment areas larger than 10 km^2; $U(t)$ is the unit hydrograph (1/h); α is the distribution factor for fast and slow cascade (−). k_1, k_2 is the storage coefficients for fast and slow cascade (h); L is the longest flowpath (km); J is the slope (−); *ChDe*, channel density (km/km^2).

Catchment based interflow

For the model extension of interflow, the unit hydrograph is calculated for the entire catchment with a fixed factor $\alpha = 0.18$ and $k_2 = 3.84$ h. The raster of each timestep with the effective rainfall is multiplied with α to get the proportion of the fast surface runoff and the event related interflow.

Subcatchment based interflow

For the following model extension, the process is repeated with a fixed α and factor of the slow cascade k_2 for each subcatchment (Figure 9). The subcatchments were divided at each inflow according to David and Schmalz (2020). The separate slow cascade with the interflow runoff fraction is added to the model area at each node. The effective precipitation is multiplied with α for each subcatchment, so that subcatchment-based adjusted effective precipitation is added to the model area. In Figure 9 the subcatchments and their respective calculated slow retention constants (Equation 8) and individual division factors (Equations 9 and 10) are summarized. Figure 10 contains the resulting spatially distributed interflow hydrograph for each subcatchment.

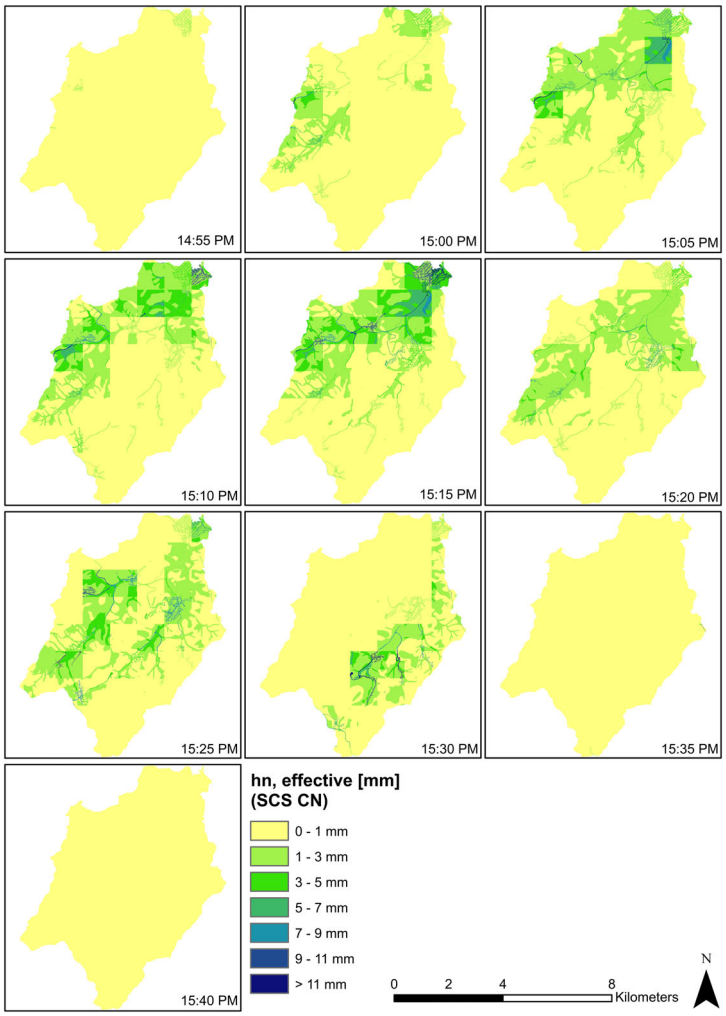

FIGURE 7 Effective rainfall (SCS-CN method) based on spatially distributed SCS-CN-values (Figure 6) and temporally invariant runoff coefficients for April 23, 2018.

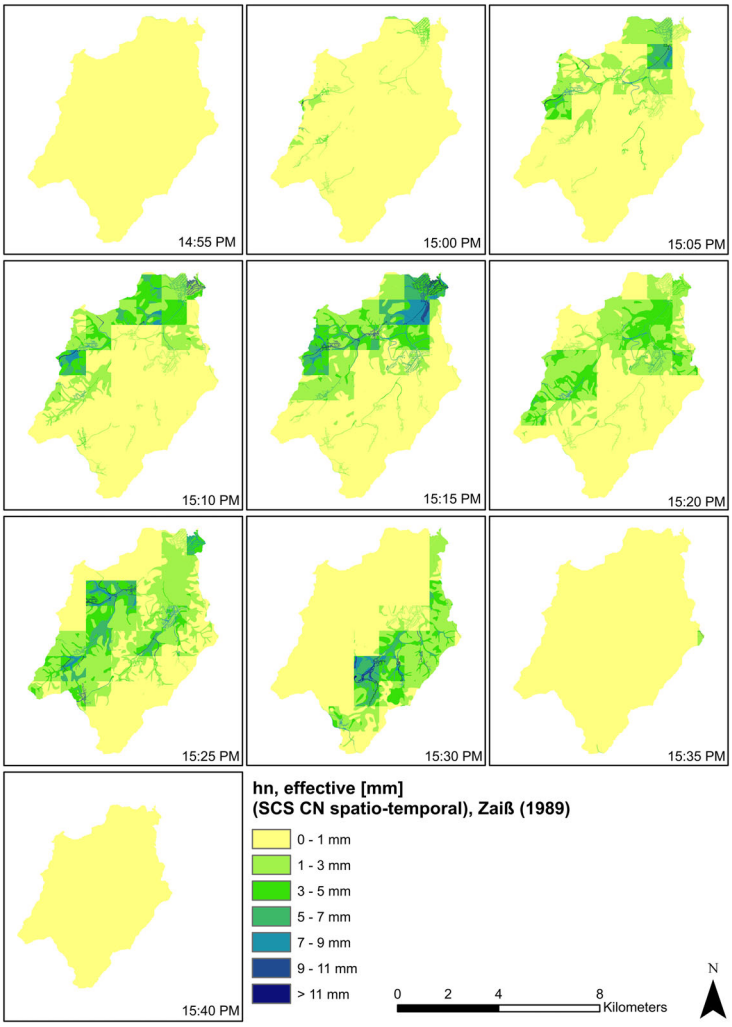

FIGURE 8 Effective rainfall (extended SCS-CN method) based on spatially distributed CN-values and temporally variable runoff coefficients for April 23, 2018.

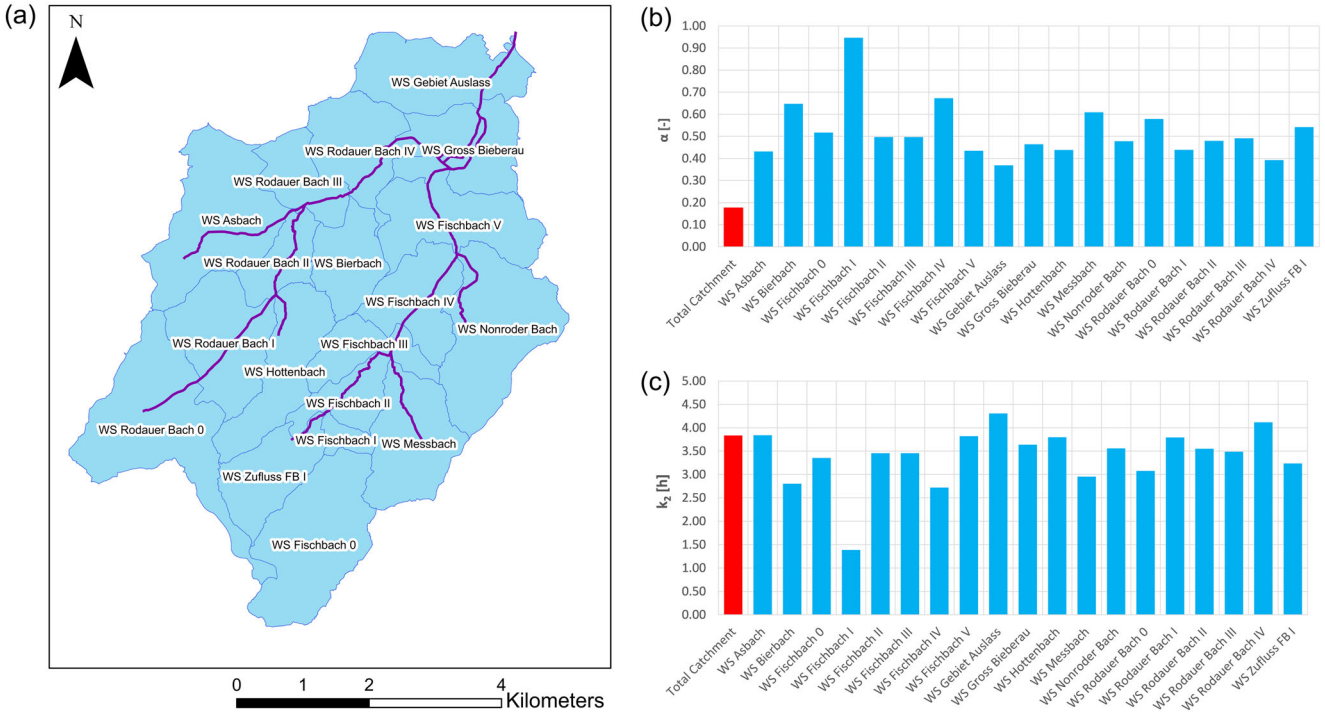

FIGURE 9 Subcatchments and parameters for conceptual interflow approach: (a) subcatchments for determination of slow cascade, (b) factor alpha α (−) to split effective rainfall in fast and slow cascade, (c) storage coefficient k_2 (h) for slow cascade.

3.7 | Procedure for the evaluation of results

The results of the noncalibrated baseline model as well as the results of the model improvements via the approach of IMI-CaHyPro are analyzed in Chapter 4 (Results and Discussion) systematically. First, there will be a detailed evaluation of the changes in the output hydrograph and distribution of effective rainfall rates due to the implemented model improvements (Chapter 4.2, Figures 11–23). Afterwards, the results of the individual model runs are evaluated on the basis of six quality criteria (Chapter 4.3, Figures 24–28). For the model calibration process, the result analysis takes place for the baseline model by the change in output hydrographs (Chapter 4.4.1 (Baseline model), Figure 29) and the change of quality criteria (Chapter 4.4.1 (Baseline model), Table 3). The same analysis is applied similarly for the calibrated IMI-CaHyPro model (Chapter 4.4.1 (IMI-CaHyPro model), Figure 30 and Table 4). The influence of the approach of IMI-CaHyPro on the parameter estimation of the calibrated IMI-CaHyPro model is analyzed in Table 5 (Chapter 4.4.2). For this purpose, the free model parameters initially assigned based on literature values to the baseline model are compared with the parameter-set of the calibrated baseline model and the parameter-set of the calibrated IMI-CaHyPro model. The evaluation of the general model results takes place based on six standardized quality criteria (Equations 14–19). The used indices are briefly presented in the following paragraph.

3.7.1 | Comparison with gauging station data GB2

Nash–Sutcliffe efficiency, NSE (–)

The *NSE* (Equation 14) is used to allow a comparison of the modeled time series (Q^t_{modeled}) with the measured time series at the gauge (Q^t_{Obs}) where $\overline{Q^t_{\text{Obs}}}$ is the mean of observed discharges. The *NSE* is criticized for overestimating the peak flow (Pappenberger et al., 2008). Since the present study focuses on the mapping of extreme events, the *NSE* can be used for comparison with the measured data.

$$\text{NSE}\,(-) = 1 - \frac{\sum_{t=1}^{T}\left(\text{Q}^t_{\text{Obs}} - \text{Q}^t_{\text{modeled}}\right)^2}{\sum_{t=1}^{T}\left(\text{Q}^t_{Obs} - \overline{\text{Q}^t_{\text{Obs}}}\right)^2} \tag{14}$$

In order to be able to determine the development and possible improvement of the model results by integrating the CaHyPro, the NSE is determined one after the other. This results in seven different analyses for NSE for the model improvement process plus the determination of NSE in the calibration process. They are summarized in Table 1. The reference observed values for all NSE indices (Q^t_{Obs}) are the discharge values from the gauging station GB2.

Delta peak flow, ΔPF (m3/s)

The deviation of the calculated maximum discharge ($\text{PF}_{\text{modeled}}$) from the measured maximum discharge (PF_{obs}) is evaluated in absolute terms and given as ΔPF (m3/s) (Equation 15). For the measured event on April 23, 2018, the maximum discharge at the gauge GB2 is 12.5 m^3/s. For the simulated events, the discharge value and the respective deviation are determined and compared after each model extension.

$$\Delta\text{PF}\left(\text{m}^3/\text{s}\right) = \text{PF}_{\text{obs}} - \text{PF}_{\text{modeled}} \tag{15}$$

Delta time of peak, ΔTP (min)

As a further criterion, the deviation of the time of occurrence of the peak flow at the gauge is evaluated. This is formed as the difference (ΔTP) of the modeled time ($\text{TP}_{\text{modeled}}$) and the observed time (TP_{obs}) and the deviation is given as delta in minutes (Equation 16).

$$\Delta\text{TP}\,(\text{min}) = \text{TP}_{\text{obs}} - \text{TP}_{\text{modeled}} \tag{16}$$

Delta direct runoff volume, ΔDV (%)

The direct runoff volume is determined in each case by subtracting a constant base flow from the total runoff hydrograph. Then, the deviation of the direct runoff of the simulated runoff hydrograph ($\text{DV}_{\text{modeled}}$) from the volume of direct runoff of the observed hydrograph (DV_{obs}) is calculated. The thus determined value for ΔDV (%) (Equation 17) is calculated in percent from the observed volume.

$$\Delta\text{DV}\,(\%) = \frac{\text{DV}_{\text{obs}} - \text{DV}_{\text{modeled}}}{\text{DV}_{\text{obs}}} * 100 \tag{17}$$

Total precipitation volume, TPV (m3)

The total precipitation volume TPV (m3) is calculated as absolute index via the total rainfall heights for each time step (h_{Ni}) and the corresponding areas (a). This index is calculated for the three different rainfall scenarios of: (1) Thiessen polygons of the baseline model, (2) hourly radar rainfall and (3) 5 min radar rainfall.

$$\text{TPV}\left(\text{m}^3\right) = \sum_i h_{\text{Ni}} * a \tag{18}$$

Effective precipitation volume, EPV (m3)

The effective precipitation volume EPV (m3) is calculated as absolute index via the effective rainfall heights for each time step ($h_{N,\text{effective},i}$) and the corresponding areas (a). This index is calculated for the different scenarios: (1) uniform SCS-CN value as mean value for the entire catchment, (2) spatially distributed SCS-CN value, (3) spatiotemporal SCS-CN value, (4) calibrated SCS-CN values for baseline model runs, and (5) calibrated SCS-CN values for integrated model runs.

$$\text{EPV}\left(\text{m}^3\right) = \sum_i h_{N,\text{effective},i} * a \tag{19}$$

In summary, the following indices (Table 1) are used for the comparison with the measured data at the gauge and the relative change of the input parameters due to iterative model improvement. The indices are determined after each step of model improvement and for the different stages of model calibration.

TABLE 1 Criteria for the evaluation of results and numbering for the different model runs

Baseline model	
NSE^1, ΔPF^1, ΔTP^1, ΔDV^1, TPV^1, EPV^1	1. Uncalibrated baseline model
Model extension of Precipitation I/II	
NSE^2, ΔPF^2, ΔTP^2, ΔDV^2, TPV^2, EPV^2	2. 1 h radar rainfall
NSE^3, ΔPF^3, ΔTP^3, ΔDV^3, TPV^3, EPV^3	3. 5 min radar rainfall
Model extension of Runoff formation I/II	
NSE^4, ΔPF^4, ΔTP^4, ΔDV^4, TPV^4, EPV^4	4. Spatial SCS-CN values
NSE^5, ΔPF^5, ΔTP^5, ΔDV^5, TPV^5, EPV^5	5. Spatiotemporal SCS-CN values
Model extension of Interflow I/II	
NSE^6, ΔPF^6, ΔTP^6, ΔDV^6, TPV^6, EPV^6	6. Catchment based interflow
NSE^7, ΔPF^7, ΔTP^7, ΔDV^7, EPV^7, EPV^7	7. Subcatchments based interflow
Calibration process	
NSE, ΔPF, ΔTP, ΔDV, TPV, EPV[a]	8. Calibration runs of *Baseline model*
NSE, ΔPF, ΔTP, ΔDV, TPV, EPV[a]	9. Calibration runs of *IMI-CaHyPro model*

Note: In Section 4, the abbreviations and notations are used according to this table.

[a]The results of the baseline model are presented in Table 3 and for the IMI-CaHyPro model in Table 4. Since there are several model runs, they are not distinguished again with an abbreviation.

3.7.2 | Comparison of model parametrization after calibration

The effect of the approach of IMI-CaHyPro on the finally calibrated model parameters of runoff formation (SCS-CN values) and runoff concentration (Manning's n value) is evaluated. For this comparison, the three parameter sets: 1. Baseline model, 2. Calibrated Baseline model, and 3. Calibrated IMI-CyHyPro model are compared. The notation according to Table 2 will be used.

TABLE 2 Evaluated parameter sets after calibration routine.

CN_{Baseline} n_{Baseline}	1. Initial parameter set for uncalibrated baseline model
$CN_{\text{Baseline,calibrated}}$ $n_{\text{Baseline, calibrated}}$	2. Parameter set for calibrated baseline model
$CN_{\text{IMI-CaHyPro}}$ $n_{\text{IMI-CaHyPro}}$	3. Parameter set for calibrated IMI-CaHyPro model

4 | RESULTS AND DISCUSSION

4.1 | Baseline model

The uncalibrated baseline model shows a temporally delayed runoff peak and a significantly too low effective precipitation and direct runoff (Figure 10). The effective precipitation results from the amount of input precipitation (Figure 11) associated with runoff losses due to initial parametrization of runoff formation. Therefore, the excessively low direct runoff can result either from the input precipitation being too low or from the SCS-CN values not being calibrated. The difference between effective input precipitation and direct runoff at the gauging station can be attributed to losses due to sinks and depressions in the unfilled terrain model. The poor correspondence of the model results with the measured data is also reflected by the quality criterion of the $NSE^1 = -0.36$ (For notations of the result analysis of the model runs, see Table 1).

4.2 | Results of iterative model improvement

4.2.1 | Precipitation

One hour radar rainfall

The model extension with spatially distributed input precipitation and unchanged parameterization of the

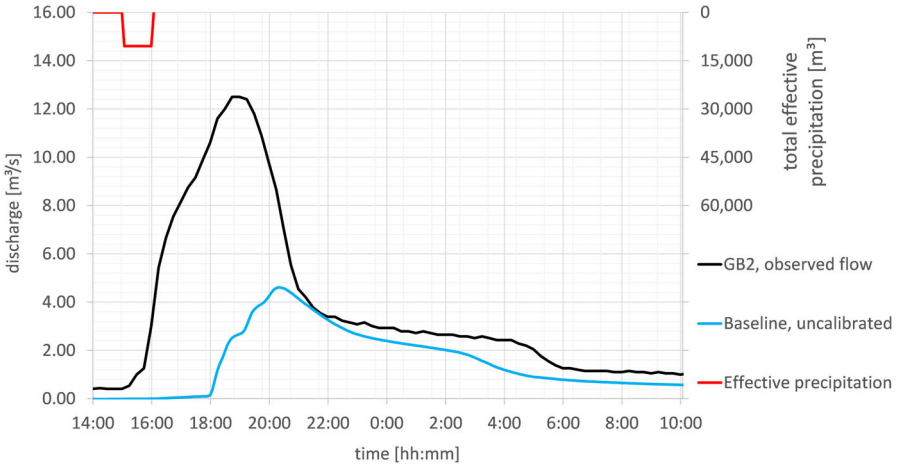

FIGURE 10 Simulated hydrograph and effective precipitation of uncalibrated baseline model in comparison to observed flow at GB2.

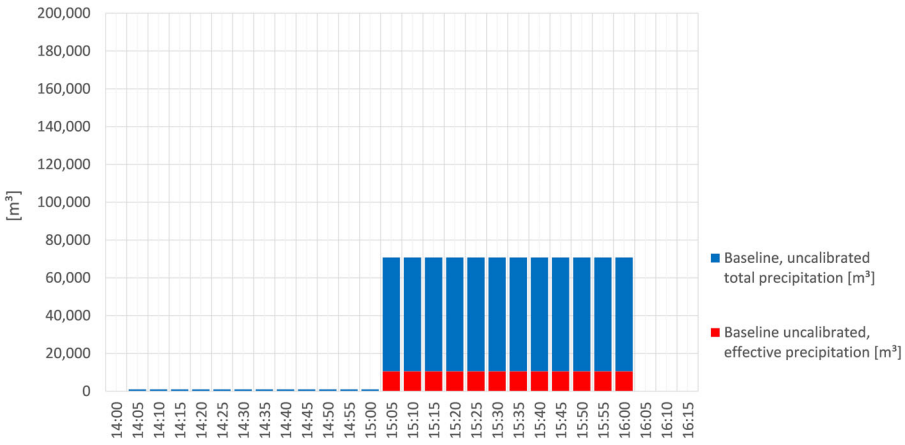

FIGURE 11 Input and effective precipitation data of uncalibrated baseline model.

runoff formation shows a faster increase of the hydrograph at the gauging station (Figure 12). In addition, a significant increase in input precipitation is detected, resulting in increased direct runoff at the gauging station. The effective precipitation (Figure 13) and the direct runoff volume continue to be significantly lower than the measured data. There is little time lag in the peak discharge compared to the measured discharge values. The significantly better agreement of the model results due to the spatially distributed input precipitation is also reflected in a significant improvement of the NSE to $NSE^2 = 0.65$.

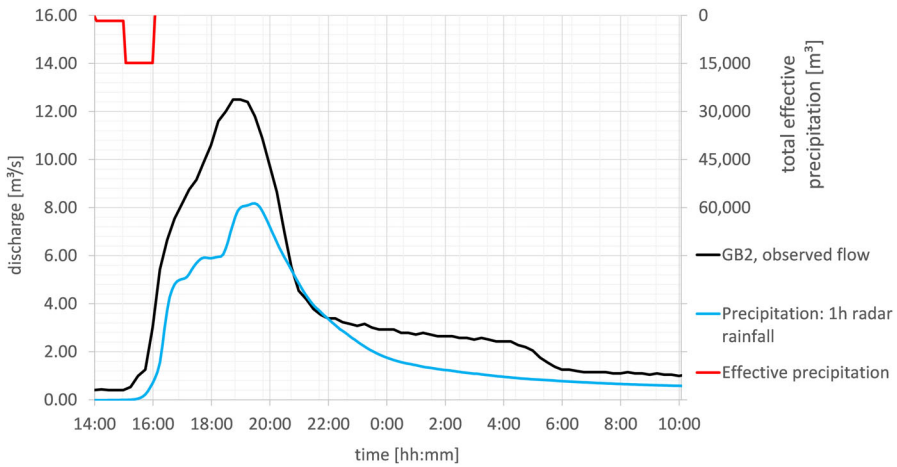

FIGURE 12 Simulated hydrograph and effective precipitation of model improvement with 1 h radar rainfall in comparison to observed flow at GB2.

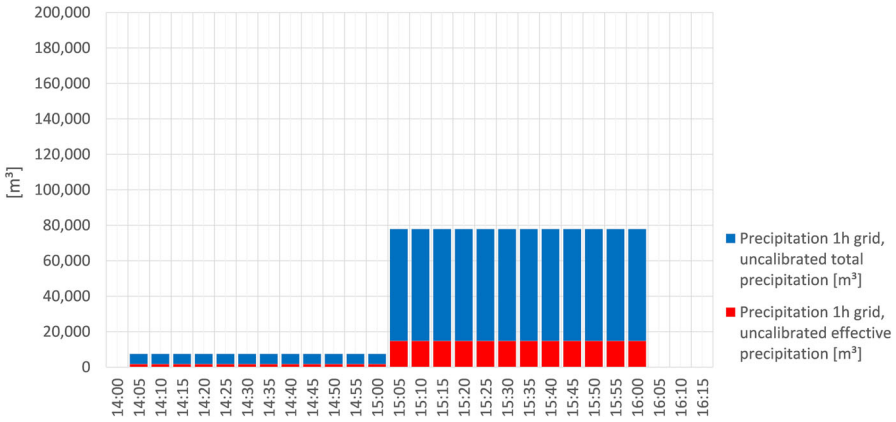

FIGURE 13 Input and effective precipitation data of model improvement with 1 h radar rainfall.

Five minutes radar rainfall

The model extension of a spatially distributed precipitation with a temporal resolution of 5 min results again in a faster increase of the runoff hydrograph (Figure 14). The results correspondents well with the ascending branch of the measured hydrograph. The maximum discharge occurs with a short delay compared to the measured data at the gauging station. Due to the model extension, the temporal dynamics of the discharge event can be reproduced very well. This effect can be explained due to the change of temporal resolution of input precipitation data with higher and earlier effective precipitation rates (Figure 15). The improvement of the model results by adding a spatio-temporally finely resolved input precipitation is shown by an increase of the NSE. This is at $NSE^3 = 0.67$. However, the calculated discharge quantities are still too low.

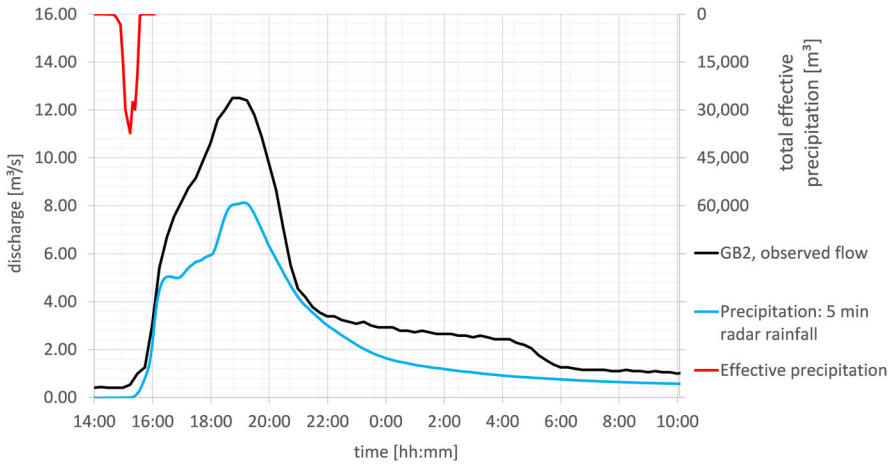

FIGURE 14 Simulated hydrograph and effective precipitation of model improvement with 5 min radar rainfall in comparison to observed flow at GB2.

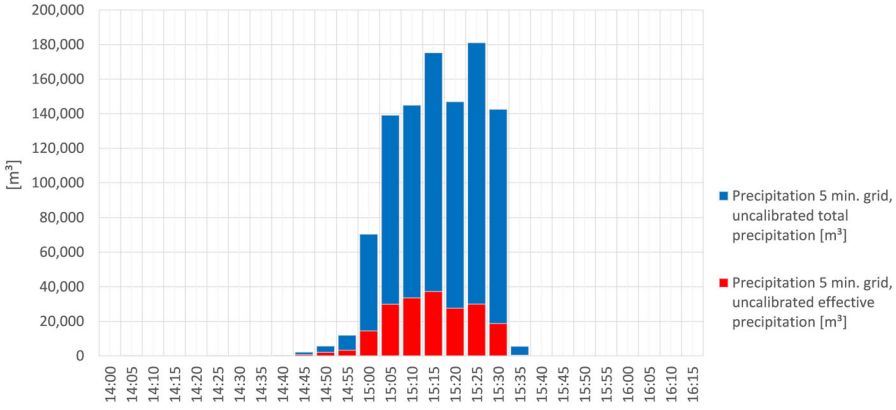

FIGURE 15 Input and effective precipitation data of model improvement with 5 min radar rainfall.

4.2.2 | Runoff formation

Spatial SCS-CN values

The model extension of spatially distributed SCS-CN values and resulting runoff coefficients leads to a faster runoff response of the catchment at the gauging station (Figure 16). This results in a faster and higher increase of the discharge hydrograph. This effect is explained due to a more realistic coupling of the runoff effective areas to the stream course and thus higher effective precipitation rates (Figure 17). The model extension shows again an improvement of the agreement of the model results with the measured data. The NSE increases to $NSE^4 = 0.72$.

Spatiotemporal SCS-CN values

By further adding a temporally distributed calculation of runoff formation, the effective precipitation increases significantly. The direct runoff volume increases by 27% compared to a purely spatially distributed runoff formation. The temporal dynamics of the runoff event is maintained

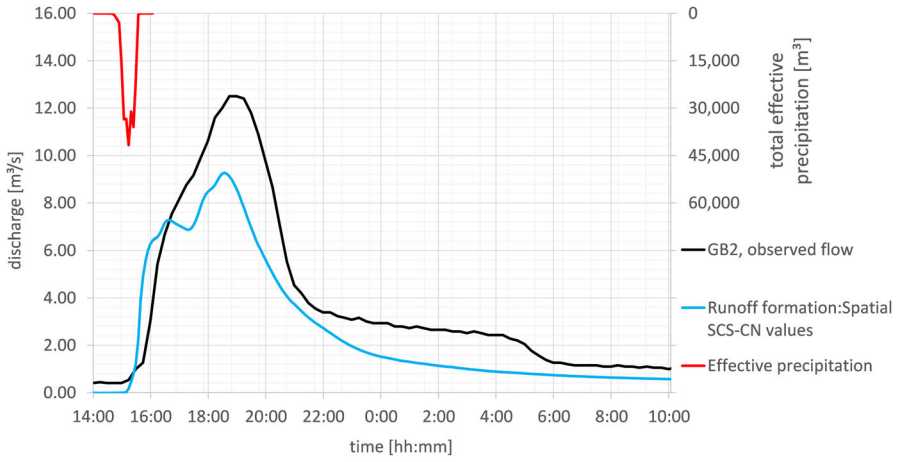

FIGURE 16 Simulated hydrograph and effective precipitation of model improvement with spatially distributed SCS-CN values in comparison to observed flow at GB2.

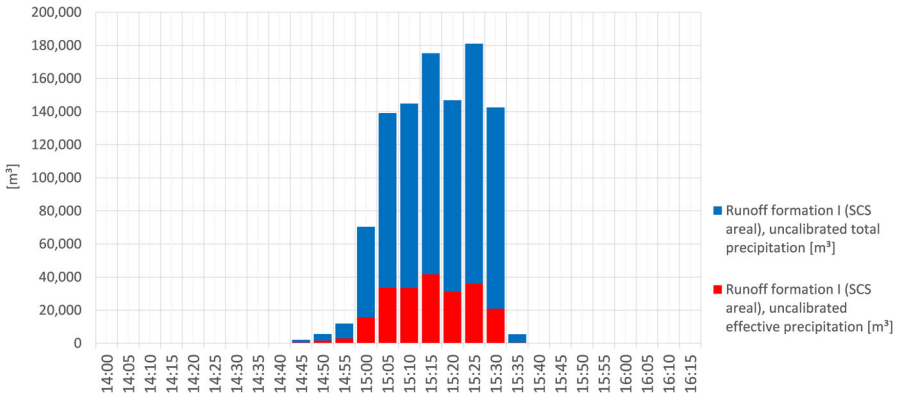

FIGURE 17 Input and effective precipitation data of model extension with spatially distributed SCS-CN values.

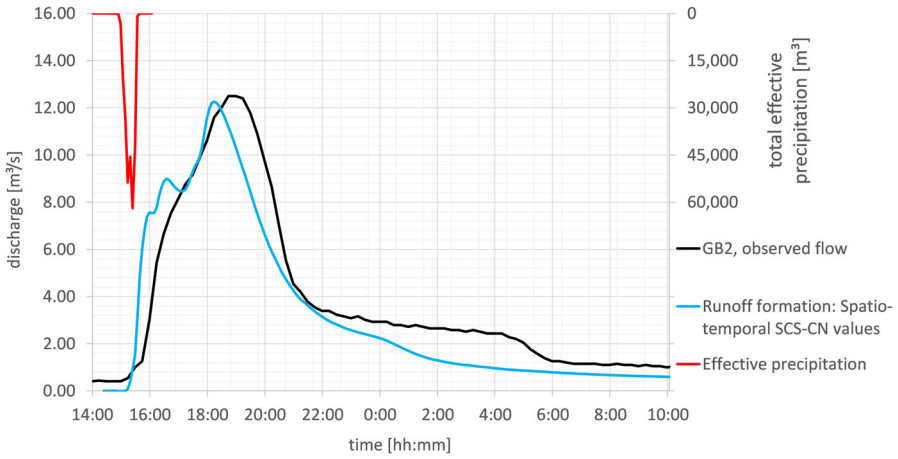

FIGURE 18 Simulated hydrograph and effective precipitation of model improvement with spatiotemporal SCS-CN values in comparison to observed flow at GB2.

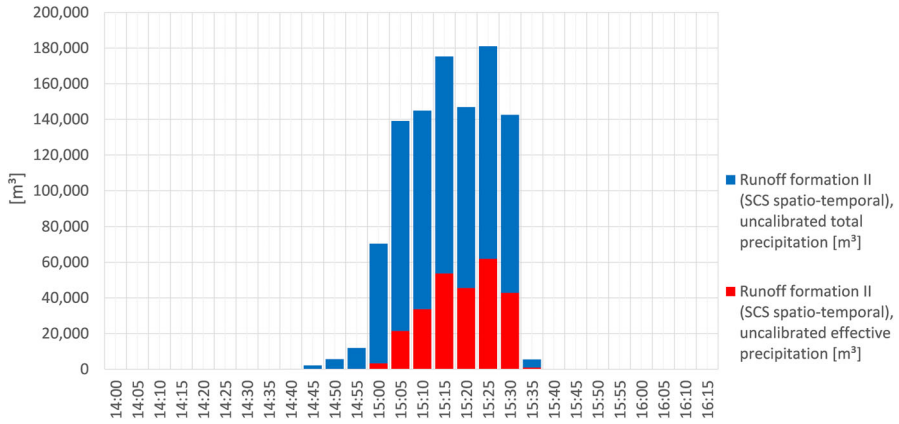

FIGURE 19 Input and effective precipitation data of model extension with spatiotemporal SCS-CN values.

(Figure 18). While the total precipitation is equally distributed as in the previous simulation, the temporal dynamics of the effective precipitation changes significantly. At the beginning of the event, the impulses of the effective precipitation are lower than in the case of the temporally independent runoff formation. Toward the end of the event, effective precipitation increases and is higher than those from the simulation with a temporally constant runoff coefficient (Figure 19). This corresponds to a better representation of the catchment soil conditions during the event. In addition, losses due to depressions, swales, interception, wetting, etc. are reduced during the precipitation event, which in turn leads to an increasing runoff coefficient during the event. The increase in runoff volume due to the implementation of a time-dependent runoff formation process leads to a significant improvement of the model results. The NSE increases to $NSE^5 = 0.83$.

4.2.3 | Interflow

Catchment based interflow

By implementing the process of interflow, the simulated runoff dynamics change significantly. While the time of the occurrence of the flood peak is preserved, the peak discharge is strongly reduced. The hydrograph flattens considerably and the concentration time of the falling branch increases significantly (Figure 20). A partitioning factor of $\alpha = 0.18$ was calculated as initial parametrization for the entire catchment area, so that the major part of the precipitation runs off as interflow (Figure 21). The model's representation of the catchment's runoff dynamics is significantly degraded by this model extension with respect to this heavy rainfall event. The quality criterion NSE decreases to $NSE^6 = 0.63$.

Subcatchment based interflow

The implementation of a spatially distributed interflow results in a comparable calculated runoff hydrograph as the interflow uniformly distributed over the catchment. The peak discharge occurs with a time delay and is still clearly below the actual flood maximum (Figure 22). It can be seen that by adding the interflow, the storage coefficients and resulting concentration times are significantly overestimated. For the intermediate runoff, the mean value of the distribution of all subcatchments is at $\alpha = 0.53$ which results in a higher proportion of surface runoff in comparison to event-related interflow (Figure 23). The poor agreement of the model results due to the

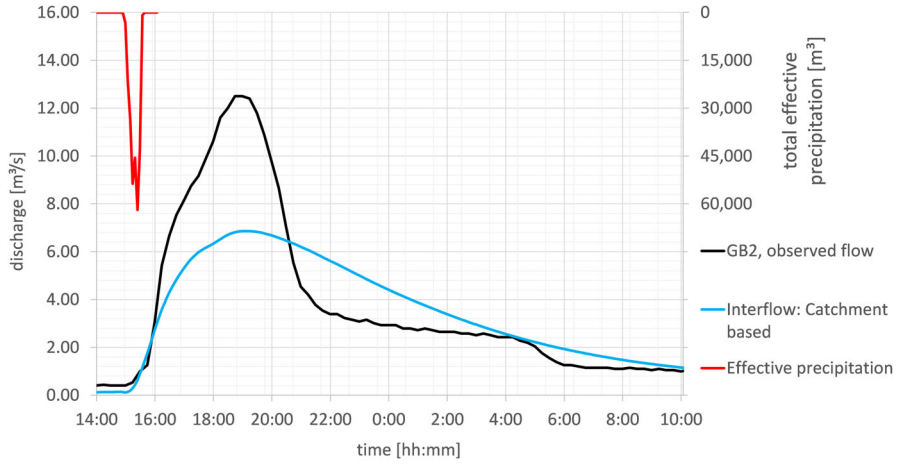

FIGURE 20 Simulated hydrograph and effective precipitation of model improvement with catchment based interflow in comparison to observed flow at GB2.

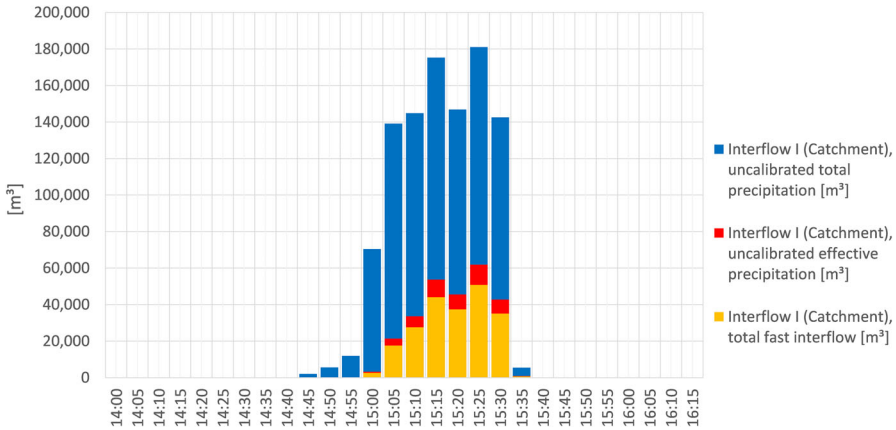

FIGURE 21 Input and effective precipitation data and proportion of interflow of model extension with catchment based interflow.

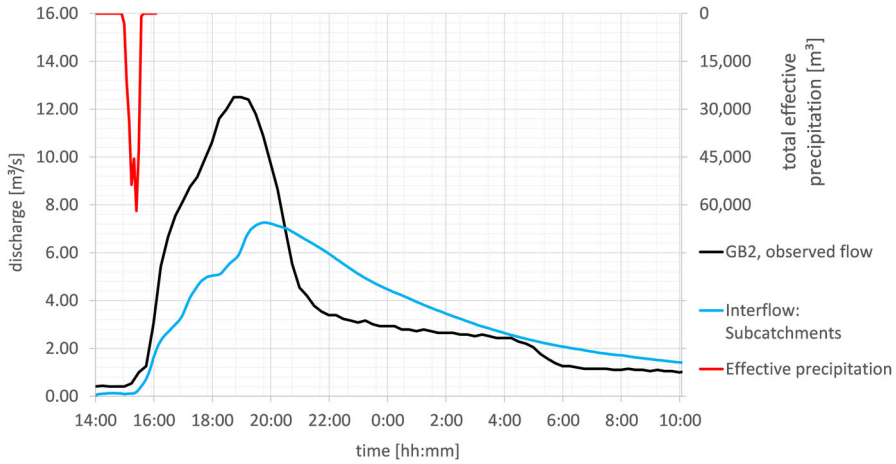

FIGURE 22 Simulated hydrograph and effective precipitation of model improvement with spatially distributed interflow in comparison to observed flow at GB2.

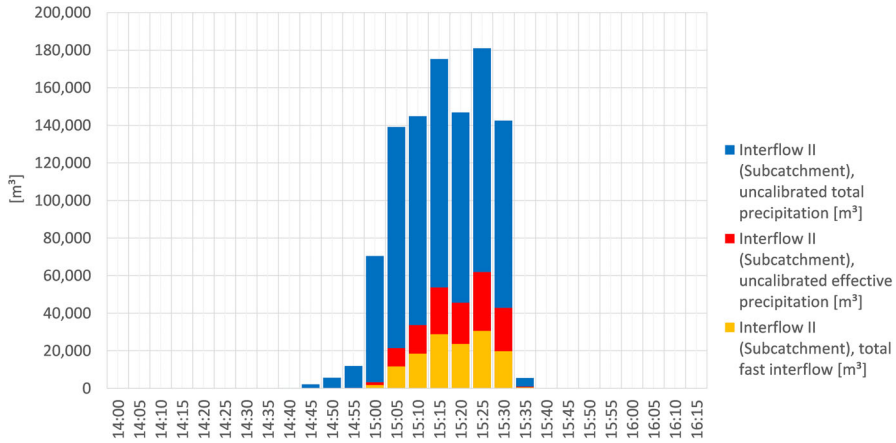

FIGURE 23 Input and effective precipitation data and proportion of interflow of model extension with spatially distributed interflow.

implementation of the spatially distributed interflow is reflected in the quality criterion of the NSE. This is at $NSE^7 = 0.47$.

4.3 | Comparison of uncalibrated model results

In the following five figures (Figures 24–28), the quality criteria of the uncalibrated baseline model and the model runs of the applied model improvements (Figure 3) are compared. The designation of the quality criteria is based on the notations from Table 1. It can be seen that the general model quality of the uncalibrated baseline model is the worst for all quality criteria ($NSE^1 = -0.36$). There is a significant improvement in model quality for all determined quality criteria by adding the hourly radar rainfall (1.1. 1 h radar rainfall). The further model improvement due to 5 min precipitation data (1.2. 5 min radar rainfall) is minor compared the hourly input data.

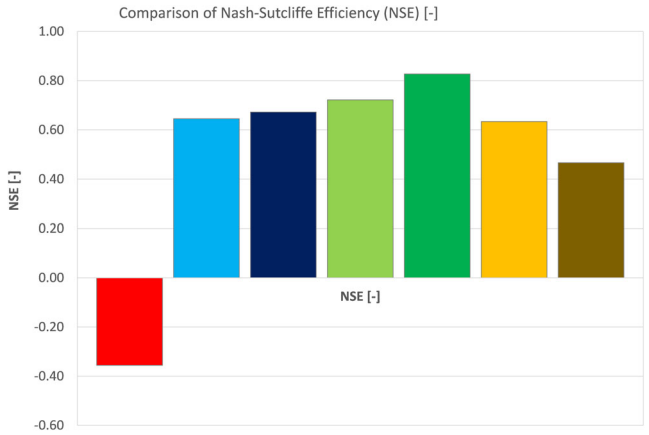

FIGURE 24 Comparison of Nash–Sutcliffe efficiency (NSE) for uncalibrated baseline model (red) and model improvements of the approach of IMI-CaHyPro*.

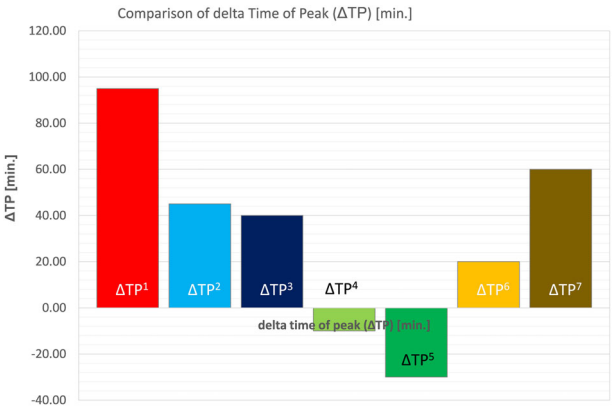

FIGURE 26 Comparison of delta time of peak (ΔTP) for uncalibrated baseline model (red) and model improvements of the approach of IMI-CaHyPro*.

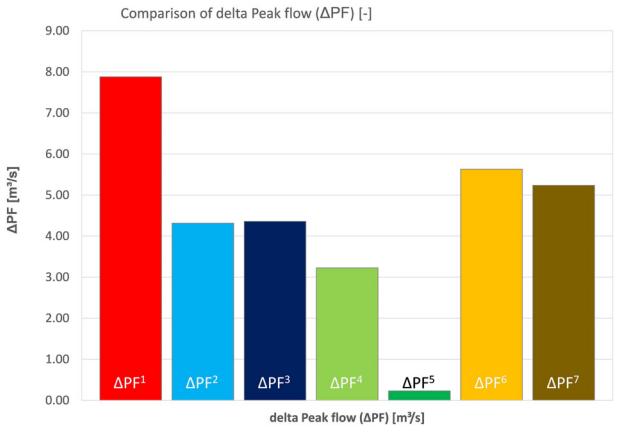

FIGURE 25 Comparison of delta peak flow (ΔPF) for uncalibrated baseline model (red) and model improvements of the approach of IMI-CaHyPro*.

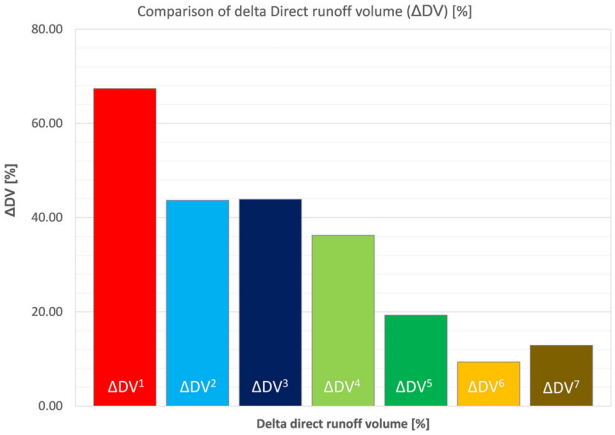

FIGURE 27 Comparison of delta direct runoff volume (ΔDV) for uncalibrated baseline model (red) and model improvements of the approach of IMI-CaHyPro*.

The integration of a spatially distributed SCS-CN values (2.1. Spatial SCS-CN values) leads to a significant improvement of the time of peak ($\Delta TP^4 = 10$ min). This effect is explainable since the runoff response of areas with higher runoff coefficients are not attenuated by an averaged runoff coefficient. By further implementing a time-dependent runoff coefficient (2.2. Spatiotemporal SCS-CN values), the NSE increases to $NSE^5 = 0.83$. In addition, the delta to the measured direct runoff volume is strongly reduced and at $\Delta DV^5 = 19\%$. It is explained due to more detailed capturing of total and effective precipitation rates. This effect is observed despite the model is still uncalibrated. Whereas the uncalibrated baseline model has a ΔDV of $\Delta DV^1 = 67\%$.

The general model quality reduces strongly due to the implementation of the additional process of interflow. The NSE decreases to $NSE^6 = 0.63$ for catchment based interflow (Interflow I) and $NSE^7 = 0.47$ for subcatchment based interflow (Interflow II). The strong flattening of the flood peak due to the delayed interflow leads to an increase of the delta peak flow to $\Delta PF^6 = 5.63$ m^3/s and $\Delta PF^7 = 5.23$. The parametrization of the interflow process took place based on literature values and simplified equation sets (Equations 6–13). The used equations of the interflow component are only dependent on the catchment characteristics but not on the characteristics of the rainfall event. This event-independent generalization of the process can cause the overestimation of storage coefficients for the short lasting storm event. The subsequent calibration and adaptation of storage coefficients to the short lasting storm event of April 23, 2018 can improve the model results even for this additional process.

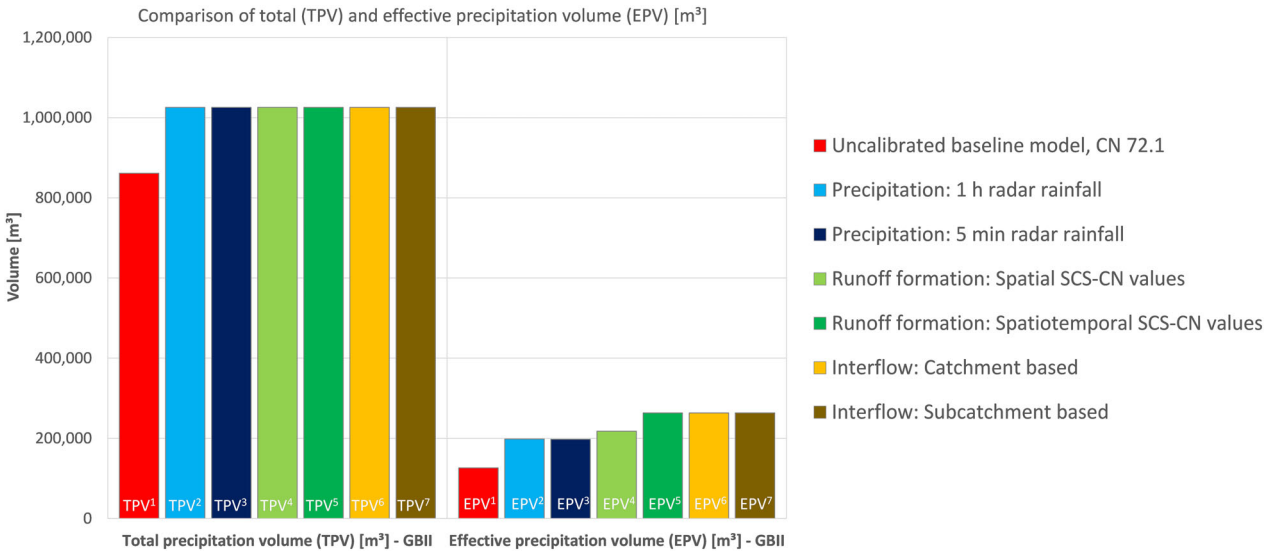

FIGURE 28 Comparison of total (TPV) and effective precipitation volume (EPV) for uncalibrated baseline model (red) and model improvements of the approach of IMI-CaHyPro*. *For notations and abbreviations of model runs, see Table 1.

4.4 | Model calibration process

4.4.1 | Comparison of hydrographs and goodness of fit parameters

Baseline model

The baseline model was manually calibrated using two parameters (SCS-CN, Manning's n). Runoff formation was calculated for SCS-CN values of 82, 85, 86, 87, and ΔDV was determined after each model run (Table 3). Manning's n values were iteratively increased/decreased for the values (+10%, −10%, −20%, −30%, −40%). The change in hydrograph was evaluated optically (Figure 29) and using the quality criteria, summarized in Table 3. The model performance increases with the increase of SCS-CN value from NSE = -0.36

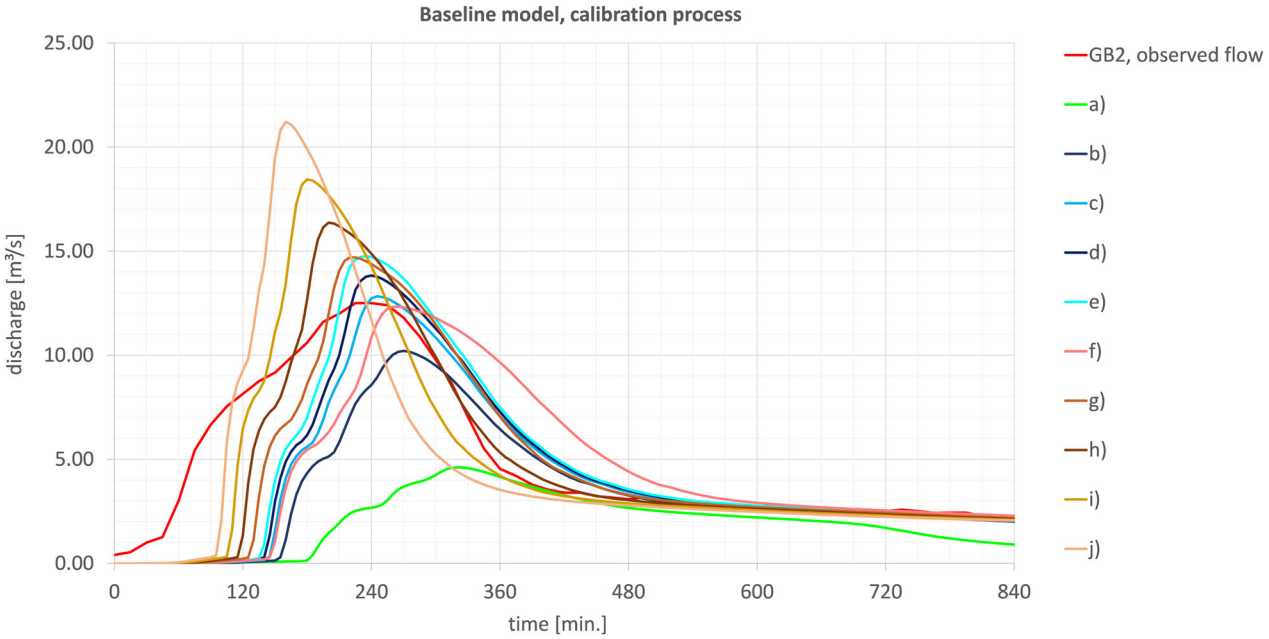

FIGURE 29 Hydrographs of calibration process of baseline model for runoff formation (CN values) and runoff delay (n values). Compare Table 3 ('Quality criteria of calibration model runs of baseline model') for model parametrization and result analysis.

TABLE 3 Quality criteria of calibration model runs of baseline model.

	Baseline[a]	CN82[b]	CN85[c]	CN86[d]	CN87[e]
Loss values					
NSE	−0.36	0.34	0.50	0.54	0.55
ΔPF	7.88	2.29	−0.34	−1.34	−2.26
ΔTP	95	45	20	15	10
ΔDV	67	29	13	7	1
TPV	861,350	861,350	861,350	861,350	861,350
EPV	126,431	228,336	273,278	291,434	310,289
	+10%[f]	**−10%[g]**	**−20%[h]**	**−30%[i]**	**−40%[j]**
Roughness values, CN = 87					
NSE	0.31	0.65	0.72	0.63	0.36
ΔPF	0.16	−2.21	−3.87	−5.96	−8.72
ΔTP	40	0	−25	−45	−65
ΔDV	2	0	−1	−2	−3
TPV	861,350	861,350	861,350	861,350	861,350
EPV	310,289	310,289	310,289	310,289	310,289

Note: (a-j) Compare runoff hydrographs in Figure 30.

(CN = 72.1) for the original baseline model to NSE = 0.55 for SCS-CN = 87. The direct runoff volume is correspondingly increased with increasing SCS-CN values. At the same time, ΔDV decreases by 66% and the time of peak is shifted forward. Nevertheless, the runoff response of the catchment occurs with a strong time delay and the ascending branch of the hydrograph is not mapped by this model parametrization. By decreasing the roughness values in the model, the response time is reduced and the flood peak increases. The NSE increases from NSE = 0.65 for 10% reduction of roughness values to NSE = 0.72 for 20% reduction of roughness values. Further reduction of roughness values again decreases the agreement with the measured data due to too high peak discharge values. In summary, the simplified set-up of the baseline model (constant runoff coefficient, station data for precipitation, no integration of interflow) cannot represent the catchment related processes for the investigated storm event. The subsequent calibration cannot compensate for the identified model deficits.

IMI-CaHyPro model

The manual calibration routine of the IMI-CaHyPro model was performed for the three processes (runoff formation, interflow, runoff concentration) based on the three parameters: SCS-CN, k_2 and n. The parameter α (interflow) was identified in advance as low sensitive and therefore not included in the calibration process. During the calibration process, the NSE serves as a benchmark for performing the subsequent calculations (Table 4). By increasing the spatially distributed SCS-CN value by 4%, ΔDV improves to 9% (NSE = 0.68). By increasing the SCS-CN value by 5%, ΔDV improves to −9% (NSE = 0.69). With further increase of CN values by 10%, ΔDV decreases to −30% (NSE = 0.64). Therefore, CN = 5% is set for the subsequent calibration of the intermediate runoff. By the catchment wide reduction of the retention constant k_2 for the slow cascades of the direct runoff (interflow), the agreement with the measured data improves considerably. The NSE increases from NSE = 0.8 for a 40% reduction of k_2 to NSE = 0.88 for a 60% reduction of k_2. At the same time ΔTP decreases to 0 min, whereas ΔPF increases to −1.3 m^3/s. The subsequent calibration of roughness values (+10%, +5%, −5%, −10%) again leads to an improvement in model performance to NSE = 0.89 for −5% and NSE = 0.90 for a 10% reduction in roughness coefficients. A qualitative analysis of the hydrographs (Figure 30) shows that in particular the calibration of the parameter for the interflow provides a significant improvement of the representation of the processes in the catchment. The initial parameterization of the velocity of the interflow was significantly underestimated for the event.

TABLE 4 Quality criteria of calibration model runs of IMI-CaHyPro model.

	IMI-CaHyPro[a]	+4%[b]	+5%[c]	+10%[d]
Loss model (SCS-CN values)				
NSE	0.47	0.68	0.69	0.64
ΔPF	5.23	3.98	2.81	0.75
ΔTP	60	45	45	25
ΔDV	13	9	−9	−30
TPV	1,025,557	1,025,557	1,025,557	1,025,557
EPV	263,355	271,950	282,665	342,375
	−40%[e]	**−50%[f]**	**−60%[g]**	**−70%[h]**
Interflow, slow component k_2, SCS-CN + 5%				
NSE	0.80	0.85	0.88	0.87
ΔPF	0.90	−0.11	−1.30	−2.70
ΔTP	25.00	15.00	0.00	−15.00
ΔDV	−11.63	1	−12	−12
TPV	1,025,557	1,025,557	1,025,557	1,025,557
EPV	282,665	282,665	282,665	282,665
	+10%[i]	**+5%[j]**	**−5%[k]**	**−10%[l]**
Roughness values, SCS-CN + 5%, k_2 − 60%				
NSE	0.81	0.84	0.89	0.90
ΔPF	0.11	−0.19	−0.91	−1.32
ΔTP	25	25	5	0
ΔDV	−12	−12	−12	−13
TPV	1,025,557	1,025,557	1,025,557	1,025,557
EPV	282,665	282,665	282,665	282,665

Note: (a-l) Compare runoff hydrographs in Figure 30.

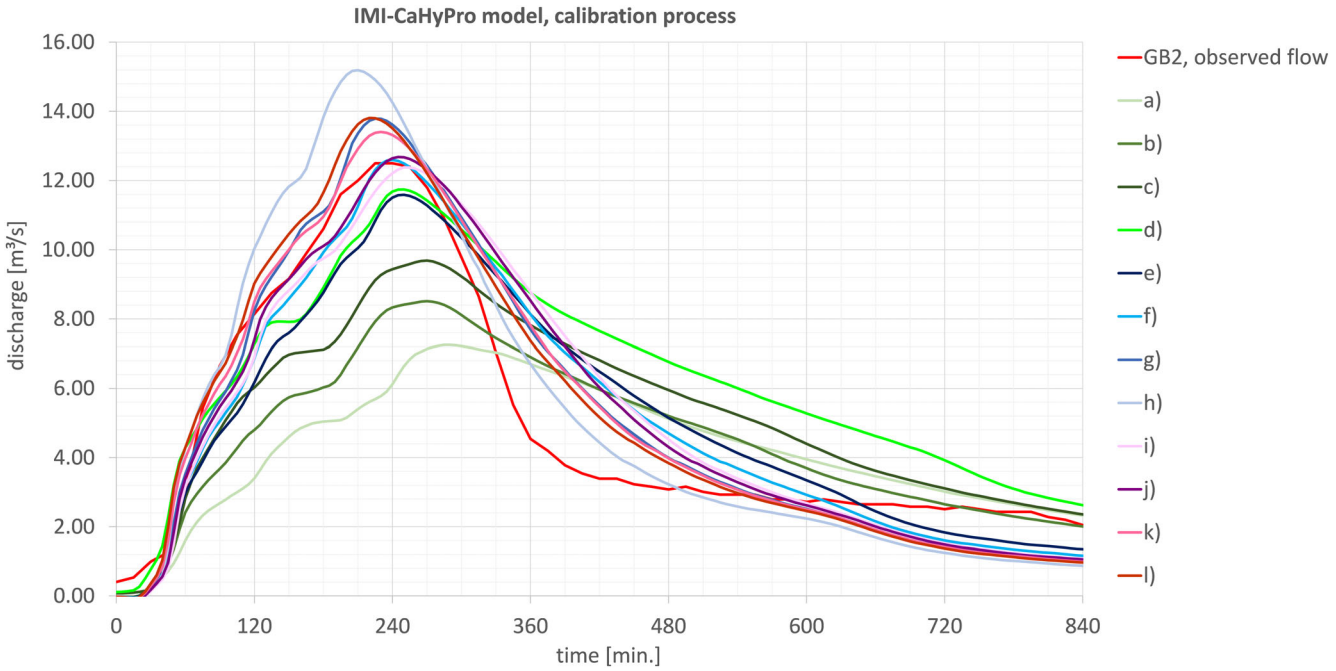

FIGURE 30 Hydrographs of calibration process of IMI-CaHyPro model for runoff formation (SCS-CN values) and runoff delay (Manning' *n* values). Compare Table 4 ('Quality criteria of calibration model runs of IMI-CaHyPro model') for model parametrization and result analysis.

4.4.2 | Comparison of model parametrization

A comparison of the calibrated parameters for the baseline model with the calibrated IMI-CaHyPro model shows that the additionally integrated CaHyPro (precipitation, runoff formation and interflow) leads to a completely different range of model parametrization. This applies in particular for the model parametrization of the SCS-CN values (Table 5). The calibrated SCS-CN value of the baseline model results in SCS-CN = 87 which is far too high for a catchment with predominantly wooded and forestry land use. The average values of the calibrated IMI-CaHyPro model results in much lower mean value of SCS-CN = 75.6. While the baseline model increased SCS-CN values by 20%, the IMI-CaHyPro approach requires only a 5% increase to calibrate the direct runoff volume at the gauging station. For the roughness coefficients, the difference between the baseline model and the IMI-CaHyPro model is 10%. In summary, it can be stated that a significant different model parameterization takes place due to the approach of IMI-CaHyPro. In this sense, the increase in SCS-CN values in the baseline model during calibration was used to compensate for the missing hydrologic processes in the catchment. Nevertheless, the results show that the calibration of the baseline model was not able to correct the model deficit.

TABLE 5 Values for initially and calibrated model parametrization of baseline model and IMI-CaHyPro model.

SCS-CN values		Manning's *n* values	
$CN_{Baseline}$	72.1	$n_{Baseline}$	0.164[a]
$CN_{Baseline,\ calibrated}$	87	$n_{Baseline,calibrated}$	0.132[a]
$CN_{IMI\text{-}CyHyPro}$	75.6[a]	$n_{IMI\text{-}CyHyPro}$	0.148[a]

[a]Mean value for total catchment.

5 | CONCLUSION AND OUTLOOK

In this study, the CaHyPro (precipitation, runoff formation and interflow) for an observed storm event were iteratively added to a simplified baseline model. After each model extension, the results were evaluated for an observed storm event based on six criteria. Subsequently, the simplified baseline model and the improved model with the developed and implemented approach of IMI-CaHyPro were manually calibrated and the effect on the subsequent model parameterization was compared. In summary, the following, key findings were made:

- The integration of spatially distributed radar-based precipitation data leads to a significant improvement of the computational results and the mapped processes.
- The reduction of the time interval of the precipitation data from 1 h to 5 min has only a minor effect on the calculation results.
- The spatiotemporal implementation of the runoff formation in the model leads to an increase of the direct runoff volume, which is of great importance for a better representation of the analyzed storm event.
- The implementation of a purely conceptual, simplified interflow approach based on two parallel cascades of linear reservoirs leads to a significant overestimation of the cascade's storage retention times. Only the calibration of the storage retention times led to an improvement of the calculation results.
- The simplified baseline model is, despite calibration, not able to well represent the fast response time of the storm event. Only with the IMI-CaHyPro approach taking into account the processes in the catchment better results are achieved.
- There is a risk to generate processes not represented in the model by calibrating free parameters of other processes. This effect leads to an overestimation of the calibrated SCS-CN values in the baseline model.

The study has shown that for storm hazard analysis in combination with the application of the DRM, the integration of CaHyPro, especially the integration of radar precipitation data in combination with a spatiotemporal parametrization of the runoff formation routine leads to better model results. These findings correspond to the ongoing research activities of the integration of radar data in existing flood forecast systems (Pfister et al., 2015; Treis & Pfister, 2019).

ACKNOWLEDGEMENTS

Our research activities are only possible through good cooperation, fruitful discussions and the provided data from state and local authorities. Our special thanks got to the DWD, HLNUG, HVBG, RP Darmstadt and the Wasserverband Gersprenzgebiet. We also thank all property owners for the opportunity to conduct investigations on their properties. We acknowledge support by the Deutsche Forschungsgemeinschaft (DFG—German Research Foundation) and the Open Access Publishing Fund of Technical University of Darmstadt. Open Access funding enabled and organized by Projekt DEAL.

DATA AVAILABILITY STATEMENT

Restrictions apply to the availability of these data, which were used under license for this study.

ORCID

Amrei David https://orcid.org/0000-0003-4684-4850
Britta Schmalz https://orcid.org/0000-0001-5961-7644

REFERENCES

Becker, A., & Glos, E. (1969). *Grundlagen der systemhydrologie*. Verlag für Bauwesen.

Bickelhaupt, M. (2018). *Photos from storm event at 23.04.2018*. Voluntary fire brigade Groß-Bieberau.

Casulli, V. (2009). A high-resolution wetting and drying algorithm for free-surface hydrodynamics. *International Journal for Numerical Methods in Fluids*, *60*(4), 391–408. https://doi.org/10.1002/fld.1896

Cea, L., & Bladé, E. (2015). A simple and efficient unstructured finite volume scheme for solving the shallow water equations in overland flow applications: The shallow water equations for overland flow applications. *Water Resources Research*, *51*(7), 5464–5486. https://doi.org/10.1002/2014WR016547

Cea, M., & Rodriguez, M. (2016). Two-dimensional coupled distributed hydrologic–hydraulic model simulation on watershed. *Pure and Applied Geophysics*, *173*(3), 909–922. https://doi.org/10.1007/s00024-015-1196-5

Costabile, P., Costanzo, C., Ferraro, D., & Barca, P. (2021). Is HEC-RAS 2D accurate enough for storm-event hazard assessment? Lessons learnt from a benchmarking study based on rain-on-grid modelling. *Journal of Hydrology*, *603*, 126962. https://doi.org/10.1016/j.jhydrol.2021.126962

David, A., & Schmalz, B. (2020). Flood hazard analysis in small catchments: Comparison of hydrological and hydrodynamic approaches by the use of direct rainfall. *Journal of Flood Risk Management*, *13*(4), e12639. https://doi.org/10.1111/jfr3.12639

David, A., & Schmalz, B. (2021). A systematic analysis of the interaction between rain-on-grid-simulations and spatial resolution in 2D hydrodynamic modeling. *Water*, *13*(17), 2346. https://doi.org/10.3390/w13172346

Deutscher Wetterdienst. (2017). *KOSTRA-DWD-2010R—Starkniederschlagshöhen für Deutschland (Bezugszeitraum 1951 bis 2010)*. Deutscher Wetterdienst (DWD) "German Weather Service".

Deutscher Wetterdienst. (2020). *Precipitation data from Reinheim station (ID: 4134), hourly data*. Deutscher Wetterdienst (DWD) "German Weather Service".

Downer, C. W., & Ogden, F. L. (2006). *Gridded Surface Subsurface Hydrologic Analysis (GSSHA) user's manual, version 1.43 for watershed modeling system 6.1*. (ERDC/CHL SR-06-1; System-Wide Water Resources Program). U.S. Army Engineer Research and Development Center.

DVWK. (1984). Arbeitsanleitung zur Anwendung von Niederschlag-Abfluß-Modellen in kleinen Einzugsgebieten. In *DVWK-Regeln zur Wasserwirtschaft (Bd. 113)*. Deutscher Verband für Wasserwirtschaft und Kulturbau e.V.

DWA. (2008). Abflüsse aus Außengebieten der Kanalisation. *Korrespondenz Abwasser, Abfall*, *2008*(8), 850–859. https://doi.org/10.3242/kae2008.08.001

European Environment Agency. (2016). *CORINE land cover (CLC) 2012*. European Environment Agency (EEA)—Copernicus—Land Monitoring Service. https://land.copernicus.eu/pan-european/corine-land-cover/clc-2012

Fraga, I., Cea, L., Puertas, J., Suárez, J., Jiménez, V., & Jácome, A. (2016). Global sensitivity and GLUE-based uncertainty analysis of a 2D–1D dual urban drainage model. *Journal of Hydrologic Engineering*, *21*(5), 04016004. https://doi.org/10.1061/(ASCE)HE.1943-5584.0001335

Grosser, P. F., & Schmalz, B. (2021). Low flow and drought in a German low mountain range Basin. *Water*, *13*(3), 316. https://doi.org/10.3390/w13030316

Guse, B., Pilz, T., Stoelzle, M., & Bormann, H. (2019). Charakterisierung und analyse hydrologischer modelle im deutschsprachigen Raum. *Wasser und Abfall*, *21*(5), 43–52. https://doi.org/10.1007/s35152-019-0043-x

Hall, J. (2015). Direct rainfall flood modelling: The good, the bad and the ugly. *Australasian Journal of Water Resources*, *19*(1), 74–85. https://doi.org/10.7158/W14-016.2015.19.1

Hessian Agency for Land Management and Geoinformation. (2017). *amtliches topographisch-kartographisches informationssystem (ATKIS®)*. Hessische Verwaltung für Bodenmanagement und Geoinformation (HVBG) "Hessian Agency for Land Management and Geoinformation".

Hessian Agency for Nature Conservation, Environment and Geology. (2017). *Digital soil map of Hesse 1:50.000 (BFD50)*. Hessisches Landesamt für Naturschutz Umwelt und Geologie (HLNUG) "Hessian Agency for Nature Conservation, Environment and Geology".

Hessian Agency for Nature Conservation, Environment and Geology. (2020a). *Precipitation data time series—Station: Modautal-Brandau-Kläranlage; ID: 2396108*. Hessisches Landesamt für Naturschutz, Umwelt und Geologie (HLNUG) "Hessian Agency for Nature Conservation, Environment and Geology".

Hessian Agency for Nature Conservation, Environment and Geology. (2020b). *Discharge time series—Station: Groß-Bieberau2 (GB2); ID: 24761005*. Hessisches Landesamt für Naturschutz, Umwelt und Geologie (HLNUG)—"Hessian Agency for Nature Conservation, Environment and Geology".

Hessisches Landesamt für Bodenmanagement und Geoinformation. (2017). *Digital Elevation Model (ATKIS® DGM)—1 m resolution*. Hessisches Landesamt für Bodenmanagement und Geoinformation (HVBG) "Hessian Agency for Land Management and Geoinformation".

Hydrologic Engineering Center. (2016). *HEC-RAS river analysis system user's manual version 5.0*. U.S. Army Corps of Engineers—Hydrologic Engineering Center (HEC).

Hydrologic Engineering Center. (2020). *HEC-RAS river analysis system hydraulic reference manual—Version 6.0 Beta*. U.S. Army Corps of Engineers—Hydrologic Engineering Center (HEC).

Hydrologic Engineering Center. (2021). *HEC-RAS river analysis system 2D modeling user's manual version 6.0*. U.S. Army Corps of Engineers—Hydrologic Engineering Center (HEC).

Hydrologic Engineering Center. (2017). *Workshop material, application of HEC-HMS using gridded precipitation in watersheds outside of the United States*. U.S. Army Corps of Engineers—Hydrologic Engineering Center (HEC).

IHWB. (2020). *Water level measurements of Groß-Bieberau, 5 min time interval*. Fachgebiet Ingenieurhydrologie und Wasserbewirtschaftung (IHWB) "Chair of Engineering Hydrology and Water Management." Department of Civil and Environmental Engineering, Technical University of Darmstadt.

Jia, Y., Shirmeen, T. A., Locke, M. E., Lizotte, R., Jr., & Douglas Shields, F., Jr. (2019). Simulation of surface runoff and channel flows using a 2D numerical model. In V. Hrissanthou & K.

Kaffas (Eds.), *Soil erosion—Rainfall erosivity and risk assessment*. IntechOpen. https://doi.org/10.5772/intechopen.80214

Kissel, M., & Schmalz, B. (2020). Comparison of baseflow separation methods in the German Low Mountain range. *Water*, *12*(6), 1740. https://doi.org/10.3390/w12061740

Pappenberger, F., Beven, K. J., Ratto, M., & Matgen, P. (2008). Multi-method global sensitivity analysis of flood inundation models. *Advances in Water Resources*, *31*(1), 1–14. https://doi.org/10.1016/j.advwatres.2007.04.009

Patt, H., & Jüpner, R. (Eds.) (Hrsg.). (2013). *Hochwasser-Handbuch: Auswirkungen und Schutz (2., neu bearb Aufl)*. Springer Vieweg.

Pfister, A., Treis, A., & Teichgräber, B. (2015). Der Einsatz von Radardaten für wasserwirtschaftliche Zwecke bei Emschergenossenschaft und Lippeverband. *Korrespondenz Wasserwirtschaft*, *2015*(2), 115–124. https://doi.org/10.3243/kwe2015.02.005

Rangari, V. A., Umamahesh, N. V., & Bhatt, C. M. (2019). Assessment of inundation risk in urban floods using HEC RAS 2D. *Modeling Earth Systems and Environment*, *5*(4), 1839–1851. https://doi.org/10.1007/s40808-019-00641-8

Schmalz, B., & Kruse, M. (2019). Impact of land use on stream water quality in the German Low Mountain Range Basin Gersprenz. *Landscape Online*, *72*, 1–17. https://doi.org/10.3097/LO.201972

Scholand, D., & Schmalz, B. (2021). Deriving the main cultivation direction from open remote sensing data to determine the support practice measure contouring. *Land*, *10*(11), 1279. https://doi.org/10.3390/land10111279

Treis, A., & Pfister, A. (2019). Flächenhafte Niederschlagserfassung mittels Radar—Erfahrungen aus 25 Jahren Radardatennutzung bei Emschergenossenschaft und Lippeverband. *Wasserwirtschaft*, *109*(7–8), 56–59. https://doi.org/10.1007/s35147-019-0190-8

USDA (Ed.) (Hrsg.). (1986). *Urban hydrology for small watersheds, technical release (TR)—55*. United States Department of Agriculture, Natural Resources Conservation Service.

Wackermann, R. (1981). Eine Einheitsganglinie aus charakteristischen Systemwerten ohne Niederschlags-Abfluß-Messungen—A unit hydrograph developed from characteristic parameters without the aid of rainfall-runoff readings. *Wasser und Boden*, *1981*(1), 23–28.

Weiler, M., McDonnell, J. J., Tromp-van Meerveld, I., & Uchida, T. (2005). Subsurface stormflow. In M. G. Anderson & J. J. McDonnell (Eds.), *Encyclopedia of hydrological sciences* (S. hsa119). John Wiley & Sons, Ltd.. https://doi.org/10.1002/0470848944.hsa119

Winterrath, T., Brendel, C., Hafer, M., Junghänel, T., Klameth, A., Lengfeld, K., Walawender, E., Weigl, E., & Becker, A. (2018a). *Radar climatology (RADKLIM) version 2017.002; gridded precipitation data for Germany: Radar-based gauge-adjusted one-hour precipitation sum (RW) (version 1, S. approx. 40 MByte per gzip compressed ascii or binary archive with monthly data) [Gzip compressed and tar packed ascii and binary]*. Deutscher Wetterdienst (DWD). https://doi.org/10.5676/DWD/RADKLIM_RW_V2017.002

Winterrath, T., Brendel, C., Hafer, M., Junghänel, T., Klameth, A., Lengfeld, K., Walawender, E., Weigl, E., & Becker, A. (2018b). *Radar climatology (RADKLIM) version 2017.002; gridded precipitation data for Germany: Radar-based quasi gauge-adjusted five-minute precipitation rate (YW) (Version 1, S. approx. 500 MByte per gzip compressed ascii or binary archive with monthly data) [Gzip compressed and tar packed ascii and binary]*. Deutscher Wetterdienst (DWD). https://doi.org/10.5676/DWD/RADKLIM_YW_V2017.002

Yu, D., & Coulthard, T. J. (2015). Evaluating the importance of catchment hydrological parameters for urban surface water flood modelling using a simple hydro-inundation model. *Journal of Hydrology*, *524*, 385–400. https://doi.org/10.1016/j.jhydrol.2015.02.040

Zaiß, H. (1989). *Simulation ereignisspezifischer Einflüsse des Niederschlag-Abfluß-Prozesses von Hochwasserereignissen kleiner Einzugsgebiete mit N-A-Modellen, Dissertation*. TH Darmstadt—Institut für Wasserbau.

Zeiger, S. J., & Hubbart, J. A. (2021). Measuring and modeling event-based environmental flows: An assessment of HEC-RAS 2D rain-on-grid simulations. *Journal of Environmental Management*, *285*(112), 125. https://doi.org/10.1016/j.jenvman.2021.112125

SUPPORTING INFORMATION

Additional supporting information can be found online in the Supporting Information section at the end of this article.

How to cite this article: David, A., Rodriguez, E. R., & Schmalz, B. (2023). Importance of catchment hydrological processes and calibration of hydrological-hydrodynamic rainfall-runoff models in small rural catchments. *Journal of Flood Risk Management*, *16*(3), e12901. https://doi.org/10.1111/jfr3.12901